

Apolipoprotein E controls cerebrovascular integrity via cyclophilin A

R. D. BELL, E. A. WINKLER, I. SINGH, A. P. SAGARE, R. DEANE, Z. WU, D. M. HOLTZMAN, C. BETSHOLTZ, A. ARMULIK, J. SALLSTROM, B. C. BERK and B. V. ZLOKOVIC

Supplementary Information

Supplementary Figure 1

Supplementary Figure 2

Supplementary Figure 3

Supplementary Figure 4

Supplementary Figure 5

Supplementary Figure 6

Supplementary Figure 7

Supplementary Figure 8

Supplementary Figure 9

Supplementary Figure 10

Supplementary Figure 11

Supplementary Figure 12

Supplementary Figure 13

Supplementary Figure 14

Supplementary Figure 15

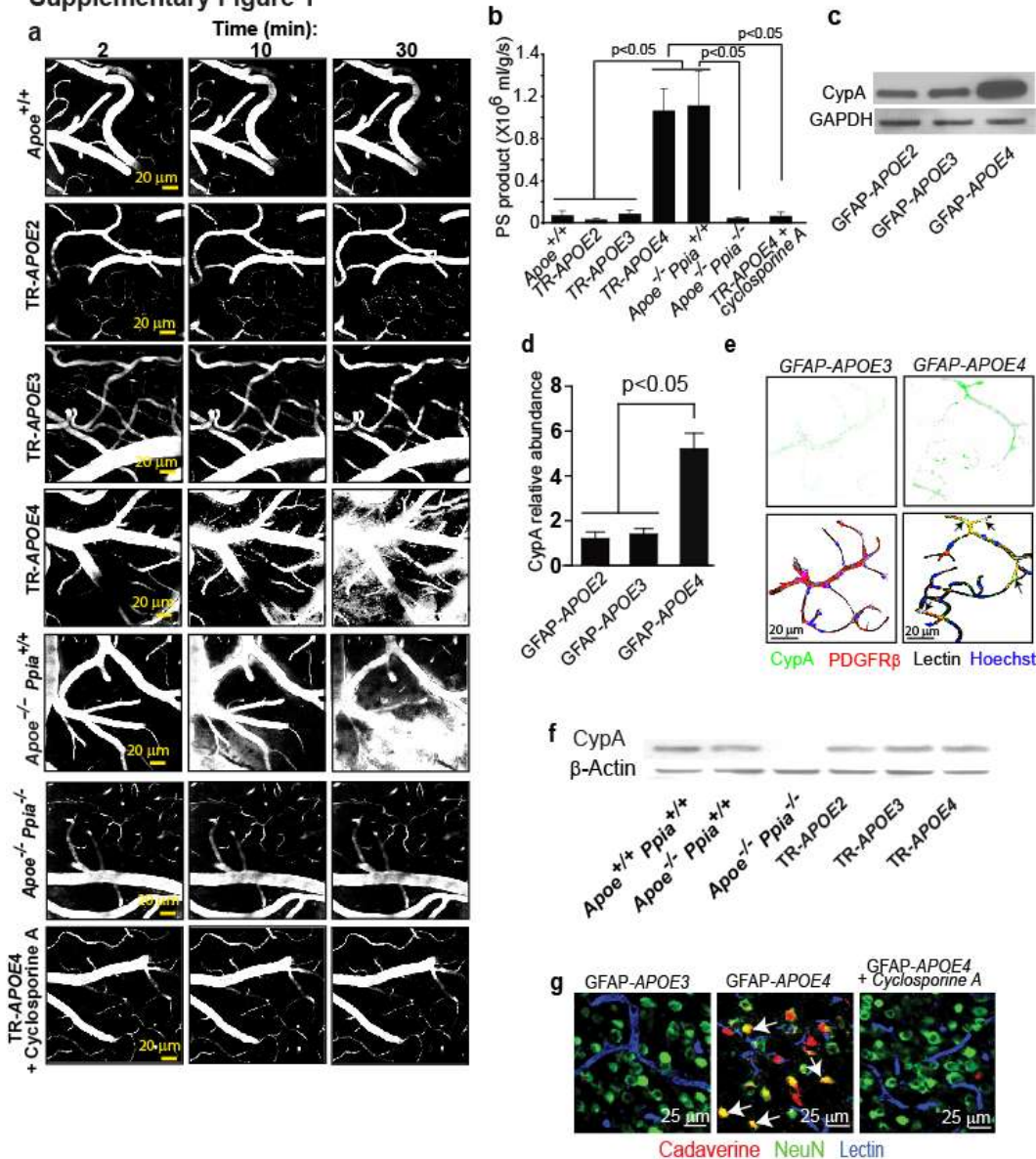
Supplementary Table 1

Supplementary Methods

Supplementary Discussion

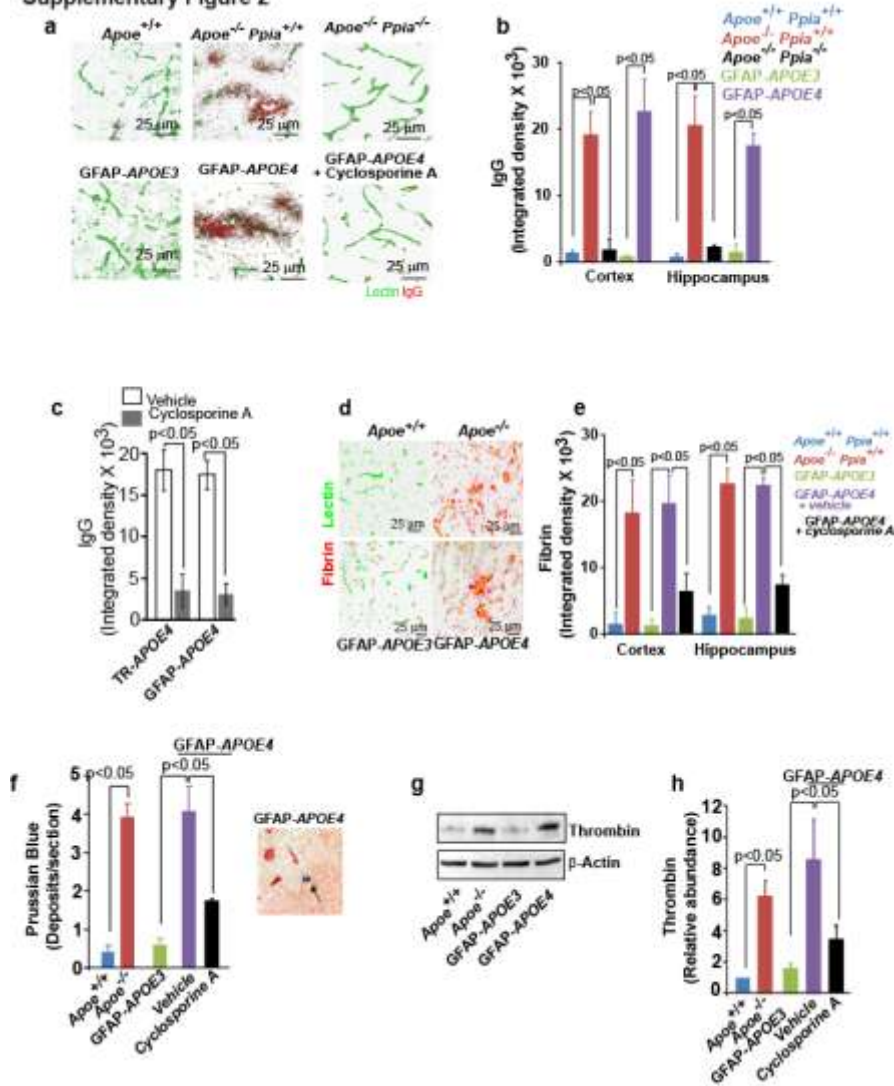
Supplementary References

Supplementary Figure 1



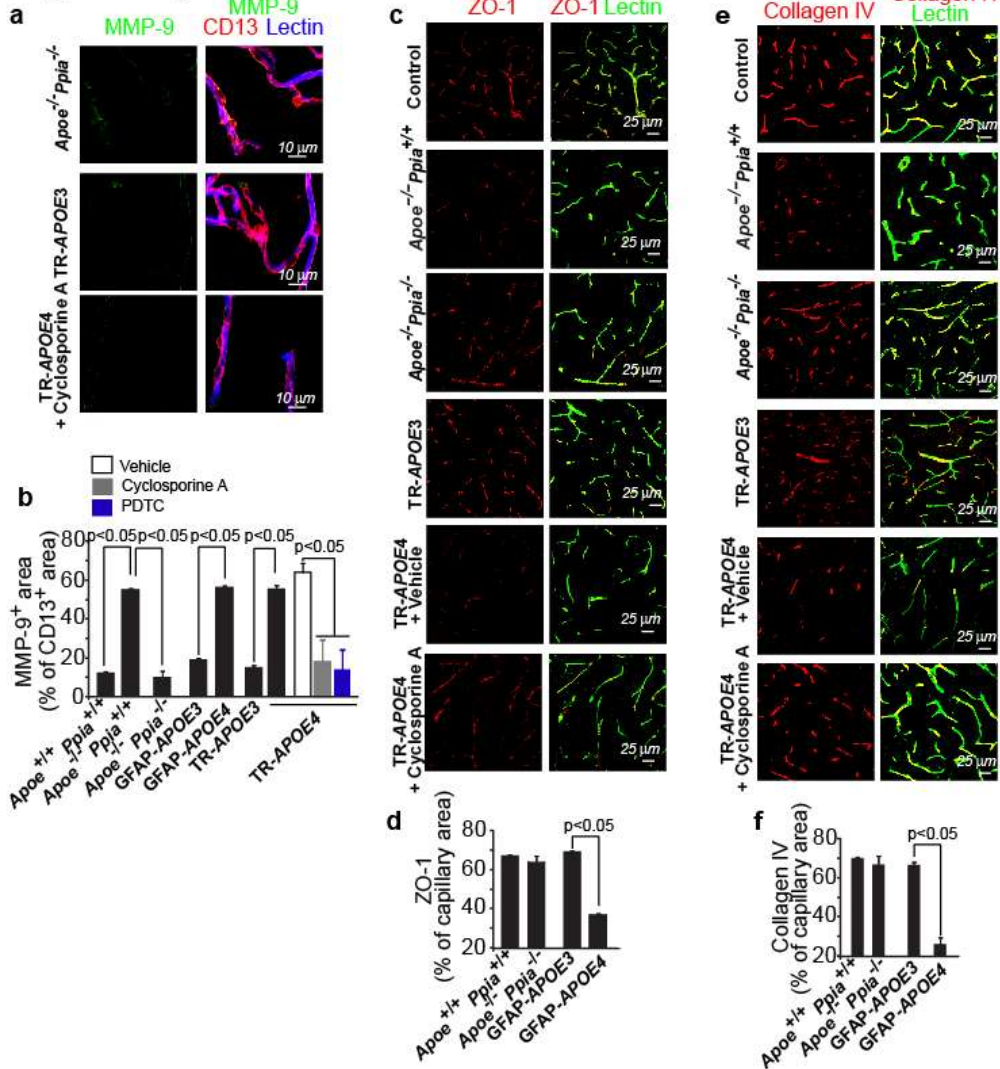
Supplementary Figure 1. BBB breakdown and increased microvascular CypA in *ApoE*^{-/-} and APOE4 transgenic mice. (a) Time-lapse multiphoton microscopy of 40 kDa TMR-Dextran (white) in cortical vessels in 6-month-old *ApoE*^{+/+} (control), TR-APOE2, TR-APOE3, TR-APOE4, *ApoE*^{-/-}*Ppia*^{+/+}, *ApoE*^{-/-}*Ppia*^{-/-} and cyclosporine A-treated TR-APOE4 mice. (b) Quantification of the permeability surface (PS) product of TMR-Dextran in the cortex of 6-month-old *ApoE*^{+/+}, TR-APOE2, TR-APOE3, TR-APOE4, *ApoE*^{-/-}*Ppia*^{+/+}, *ApoE*^{-/-}*Ppia*^{-/-} and cyclosporine A-treated TR-APOE4 mice. Mean \pm s.e.m., n=5-6 animals per group. (c) CypA immunoblotting in brain microvessels from GFAP-APOE transgenic mice. (d) Graph, CypA abundance relative to GAPDH in apoE transgenic mice. Mean \pm s.e.m., n=5-6 animals per group. (e) Low magnification confocal images of CypA (green), PDGFR β -positive pericytes (red) and lectin-positive endothelium (blue) in cortical and hippocampal microvessels isolated from *ApoE*^{+/+}, *ApoE*^{-/-} and GFAP-APOE4 mice. Yellow, colocalization of CypA with PDGFR β -positive pericytes. (f) Immunoblotting analysis of CypA in microvessel-depleted brain samples from *ApoE*^{+/+}*Ppia*^{+/+}, *ApoE*^{-/-}*Ppia*^{+/+}, *ApoE*^{-/-}*Ppia*^{-/-}, TR-APOE2, TR-APOE3 and TR-APOE4 mice. (g) Neuronal uptake (NeuN, green) of cadaverine-Alexa-Fluor-555 (red; yellow, merged) in 6-month-old GFAP-APOE4 mice and blockade with cyclosporine A. Blue, lectin-positive capillaries. d, representative results from 4-6 experiments.

Supplementary Figure 2



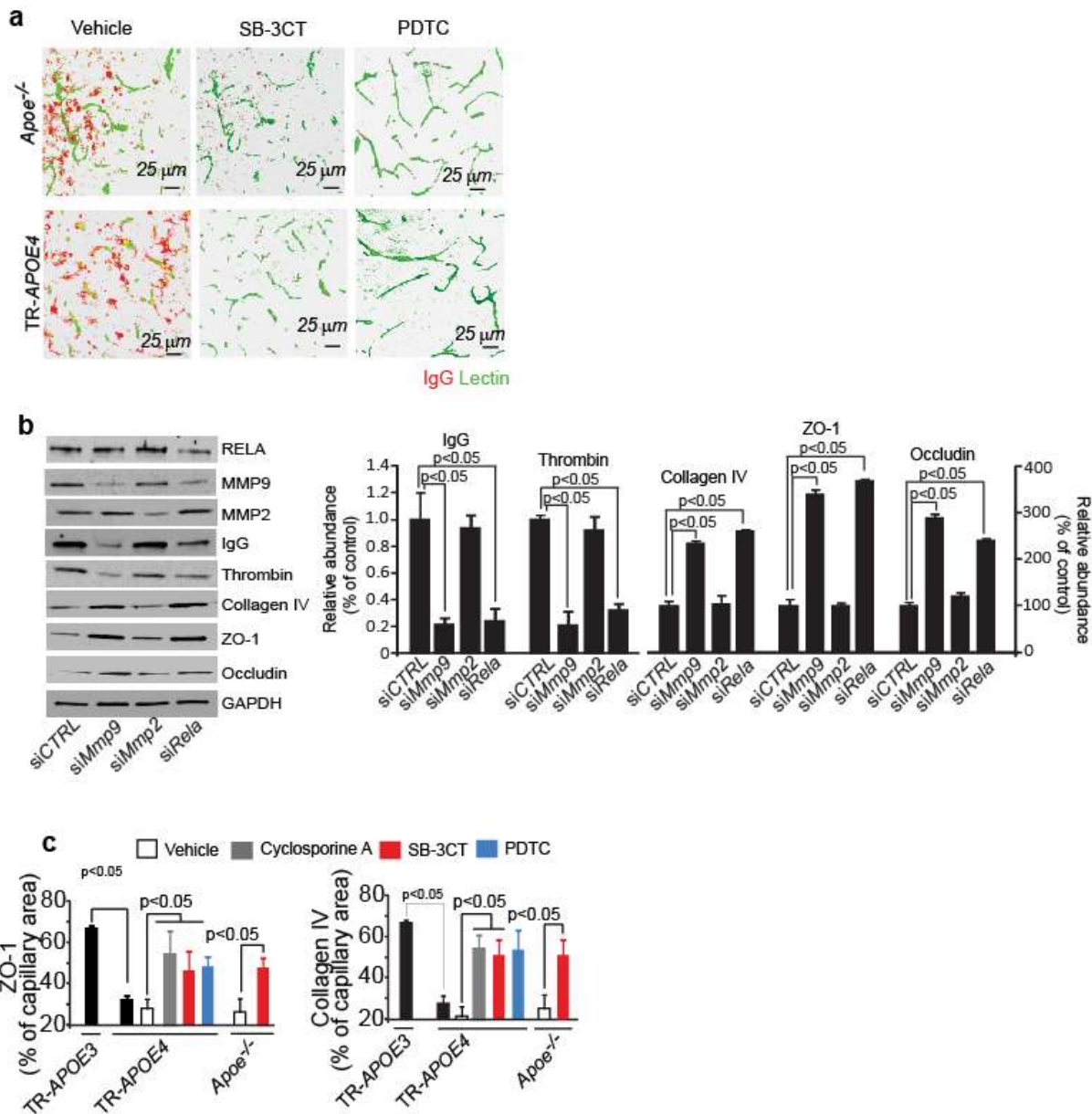
Supplementary Figure 2. Accumulation of endogenous blood-derived proteins in the brain of *ApoE*^{-/-} and *APOE4* transgenic mice. (a) Lectin-positive capillaries (green) and IgG (red) in the hippocampus of 18-month-old control, *ApoE*^{-/-} *Ppia*^{+/+}, *ApoE*^{-/-} *Ppia*^{-/-}, GFAP-*APOE3* and GFAP-*APOE4* mice untreated and cyclosporine A-treated. (b) Extravascular IgG signal intensity in the cortex and hippocampus of 18-month-old *ApoE*^{+/+} *Ppia*^{+/+}, *ApoE*^{-/-} *Ppia*^{+/+}, *ApoE*^{-/-} *Ppia*^{-/-}, GFAP-*APOE3* and GFAP-*APOE4* mice. (c) IgG signal in brains of 6-month-old TR- and GFAP-*APOE4* mice treated with vehicle or cyclosporine A (mean ± s.e.m., n=6 mice per group). (d) Confocal microscopy analysis of lectin-positive capillaries (green) and fibrin (red) in the cortex of 18-month-old *ApoE*^{+/+}, *ApoE*^{-/-}, GFAP-*APOE3* and GFAP-*APOE4* mice. Scale bar = 25 μm. (e) Quantification of extravascular fibrin deposits in the cortex and hippocampus of 18-month-old *ApoE*^{+/+} *Ppia*^{+/+}, *ApoE*^{-/-} *Ppia*^{+/+}, GFAP-*APOE3* and vehicle- or cyclosporine A-treated GFAP-*APOE4* mice. (f) Quantification of Prussian blue-positive hemosiderin deposits in sagittal brain sections containing the cortex and hippocampus of 9-month-old *ApoE*^{+/+} *Ppia*^{+/+}, *ApoE*^{-/-} *Ppia*^{+/+}, GFAP-*APOE3* and vehicle- or cyclosporine A-treated GFAP-*APOE4* mice. Inset displays a hemosiderin deposit in the cortex of a vehicle-treated GFAP-*APOE4* mouse. (g) Thrombin immunoblotting analysis in microvessel-depleted brains of 9-month-old *ApoE*^{+/+}, *ApoE*^{-/-}, GFAP-*APOE3* and GFAP-*APOE4* mice. (h) Quantification of relative thrombin abundance normalized to β-Actin in microvessel-depleted brain samples from 9-month-old *ApoE*^{+/+}, *ApoE*^{-/-}, GFAP-*APOE3* and vehicle- or cyclosporine A-treated GFAP-*APOE4* mice using densitometry analysis. In a, c, e, f and h, mean ± s.e.m., n=5-6 animals per group.

Supplementary Figure 3



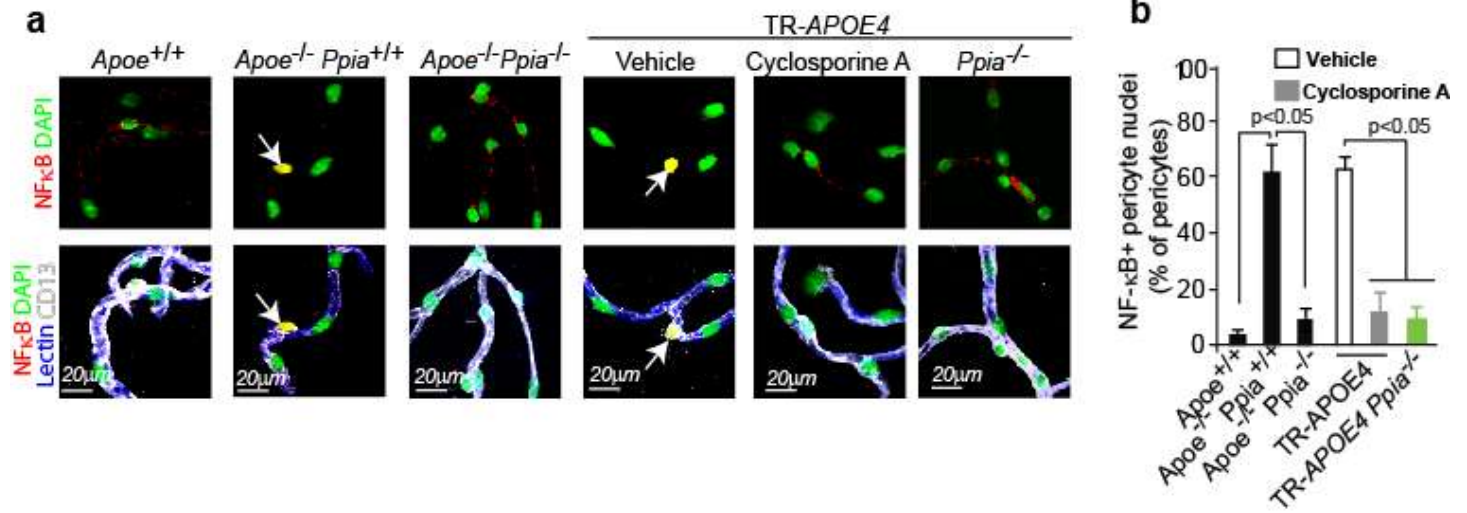
Supplementary Figure 3. MMP-9, ZO-1 and collagen IV expression in different apoE transgenic mice. (a) Confocal microscopy analysis of MMP-9 protein (green), CD13-positive pericytes (red) and lectin-positive endothelium (blue) in cortical microvessels derived from 9 month old *ApoE*^{-/-}*Ppia*^{-/-}, TR-APOE3, and TR-APOE4 mice treated with cyclosporine A. Scale bar = 10 μm. (b) Quantification of MMP-9-positive immunofluorescent signal in CD13-positive pericytes of *ApoE*^{+/+}*Ppia*^{+/+}, *ApoE*^{-/-}*Ppia*^{+/+}, *ApoE*^{-/-}*Ppia*^{-/-}, GFAP-APOE3, GFAP-APOE4, TR-APOE3 and TR-APOE4 mice treated with vehicle, cyclosporine A or PDTC. (c) Confocal microscopy analysis of ZO-1 (red) and lectin-positive microvessels (green) in the cortex of 2-week old *ApoE*^{+/+}*Ppia*^{+/+}, *ApoE*^{-/-}*Ppia*^{+/+}, *ApoE*^{-/-}*Ppia*^{-/-}, TR-APOE3, and TR-APOE4 mice treated with vehicle or cyclosporine A. Scale bar = 25 μm. (d) The percent area of lectin-positive microvessels occupied by ZO-1 immunofluorescent staining in *ApoE*^{+/+}*Ppia*^{+/+}, *ApoE*^{-/-}*Ppia*^{-/-}, GFAP-APOE3 and GFAP-APOE4 mice. (e) Confocal microscopy analysis of collagen IV (red) and lectin-positive microvessels (green) in the cortex of 2 week old *ApoE*^{+/+}*Ppia*^{+/+}, *ApoE*^{-/-}*Ppia*^{+/+}, *ApoE*^{-/-}*Ppia*^{-/-}, TR-APOE3, and TR-APOE4 treated with vehicle or cyclosporine A. Scale bar = 25 μm. (f) The percent area of lectin-positive microvessels occupied by collagen IV immunofluorescent staining in *ApoE*^{+/+}*Ppia*^{+/+}, *ApoE*^{-/-}*Ppia*^{-/-}, GFAP-APOE3 and GFAP-APOE4 mice. In b, d and f mean ± s.e.m., n=5-6 animals per group.

Supplementary Figure 4



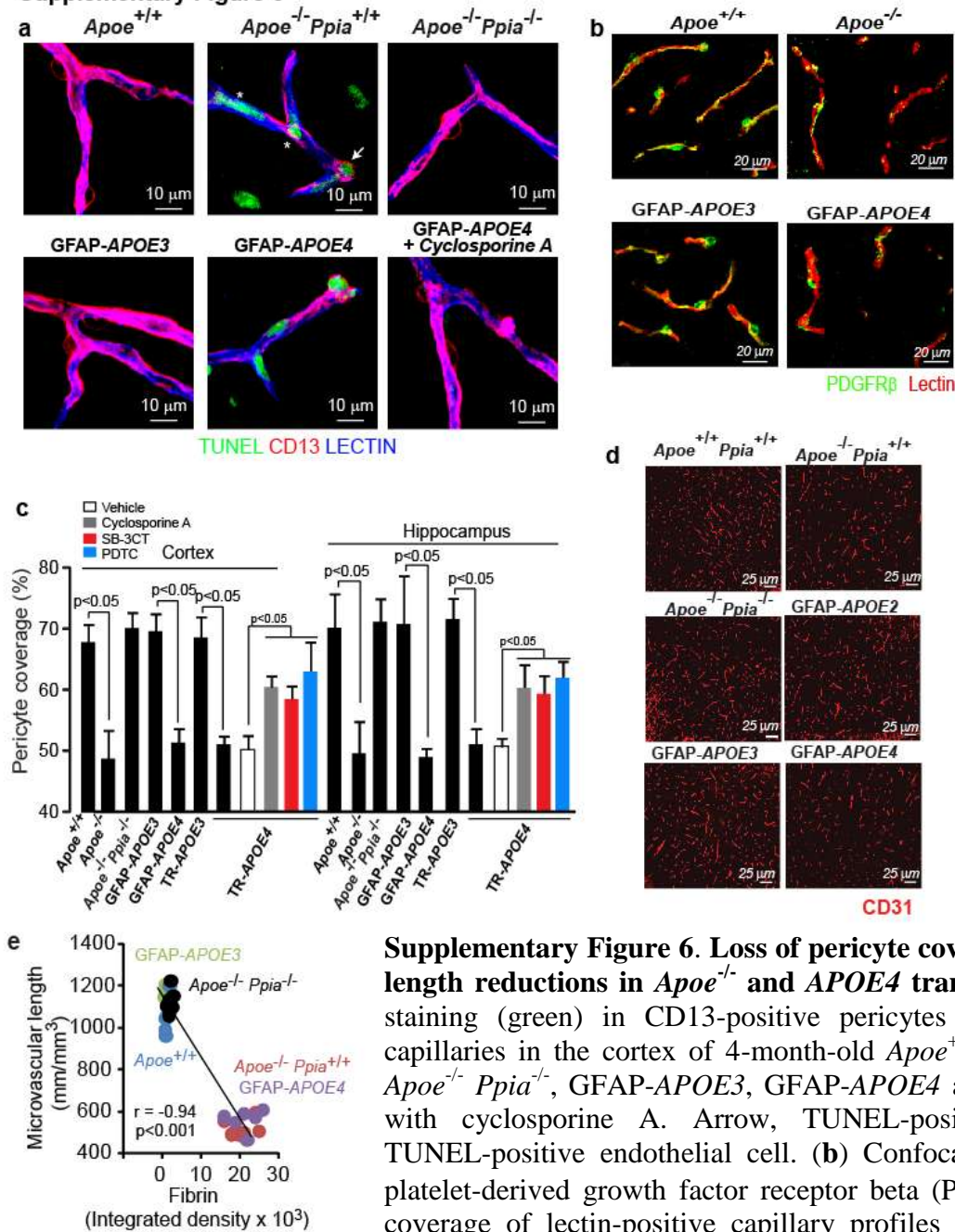
Supplementary Figure 4. The effects of pharmacological inhibition and silencing of MMP-9 and NF- κ B on blood-brain barrier integrity in *Apoe*^{-/-} and *APOE4* mice. (a) Cortical IgG (red) deposits in *Apoe*^{-/-} and TR-APOE4 mice treated with vehicle, SB-3CT or PDTC. Green, lectin-positive capillaries. Bar=25 μ m. (b) MMP-9, MMP-2 and RELA silencing with siRNA infusion into the hippocampus in 9 month-old TR-APOE4 mice. Graphs - IgG and thrombin abundance (left) and vascular ZO-1, occludin and collagen IV abundance (right) normalized to GAPDH in hippocampal samples after either control siRNA (siCTRL), *Mmp9* siRNA (siMmp9), *Mmp2* siRNA (siMmp2) or *Rela* siRNA (siRela) infusion. (c) Quantification of ZO-1 and collagen-IV immunofluorescent staining in TR-APOE3 and TR-APOE4 and *Apoe*^{-/-} mice treated with vehicle, cyclosporine A, PDTC or SB-3CT. In a, representative results from 5-6 animals per group. In b-c, mean \pm s.e.m., n=5-6 animals per group.

Supplementary Figure 5



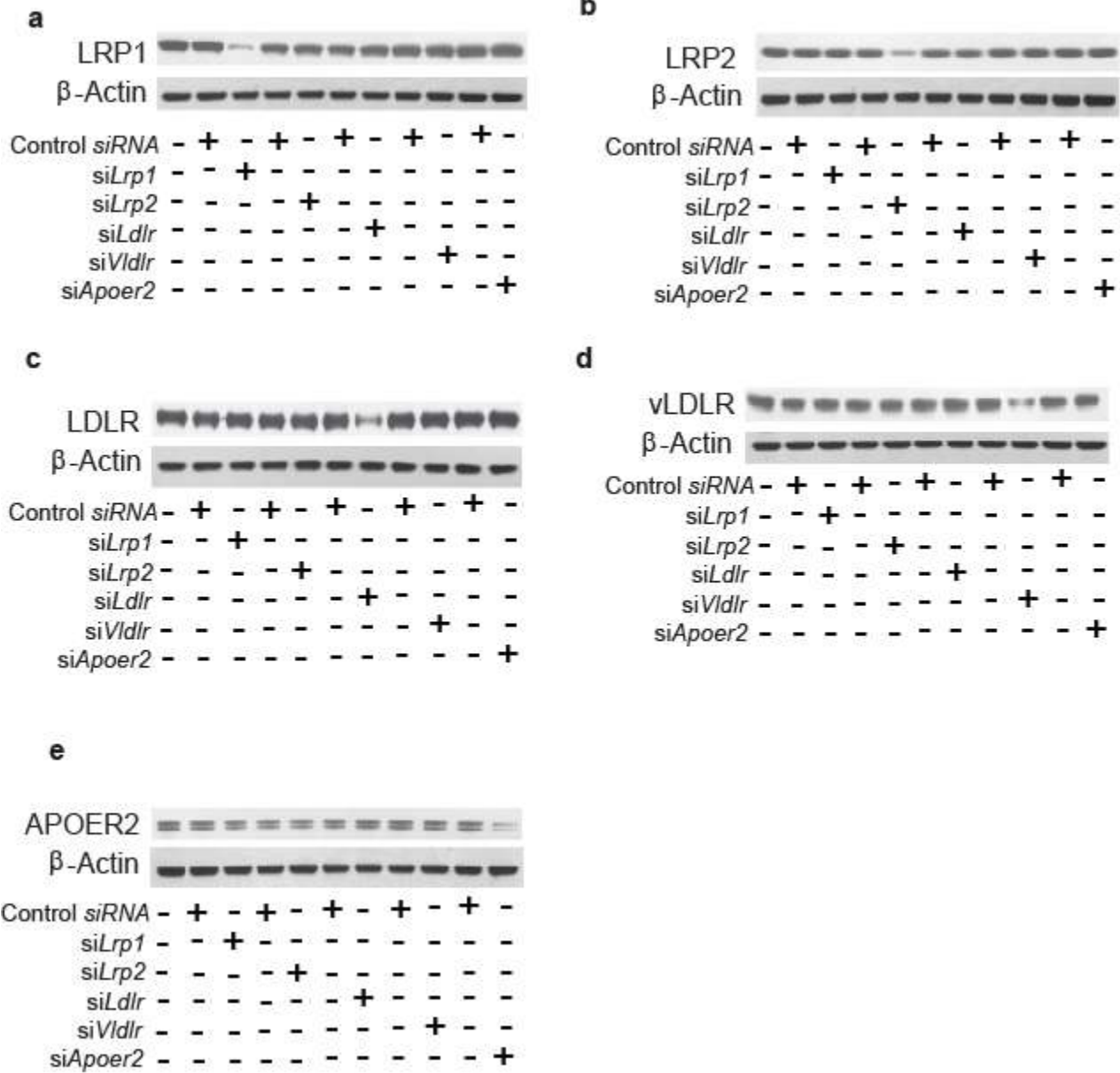
Supplementary Figure 5. NF- κ B nuclear translocation in pericytes of *Apoe*^{-/-} and *APOE4* mice. (a) NF- κ B nuclear translocation in CD13-positive pericytes on cerebral microvessels derived from *Apoe*^{-/-} and *APOE4* mice, and inhibition by CypA gene deletion and cyclosporine A. (b) Quantification of pericytes with NF- κ B-positive nuclei. In b, mean \pm s.e.m., n= 4-6.

Supplementary Figure 6



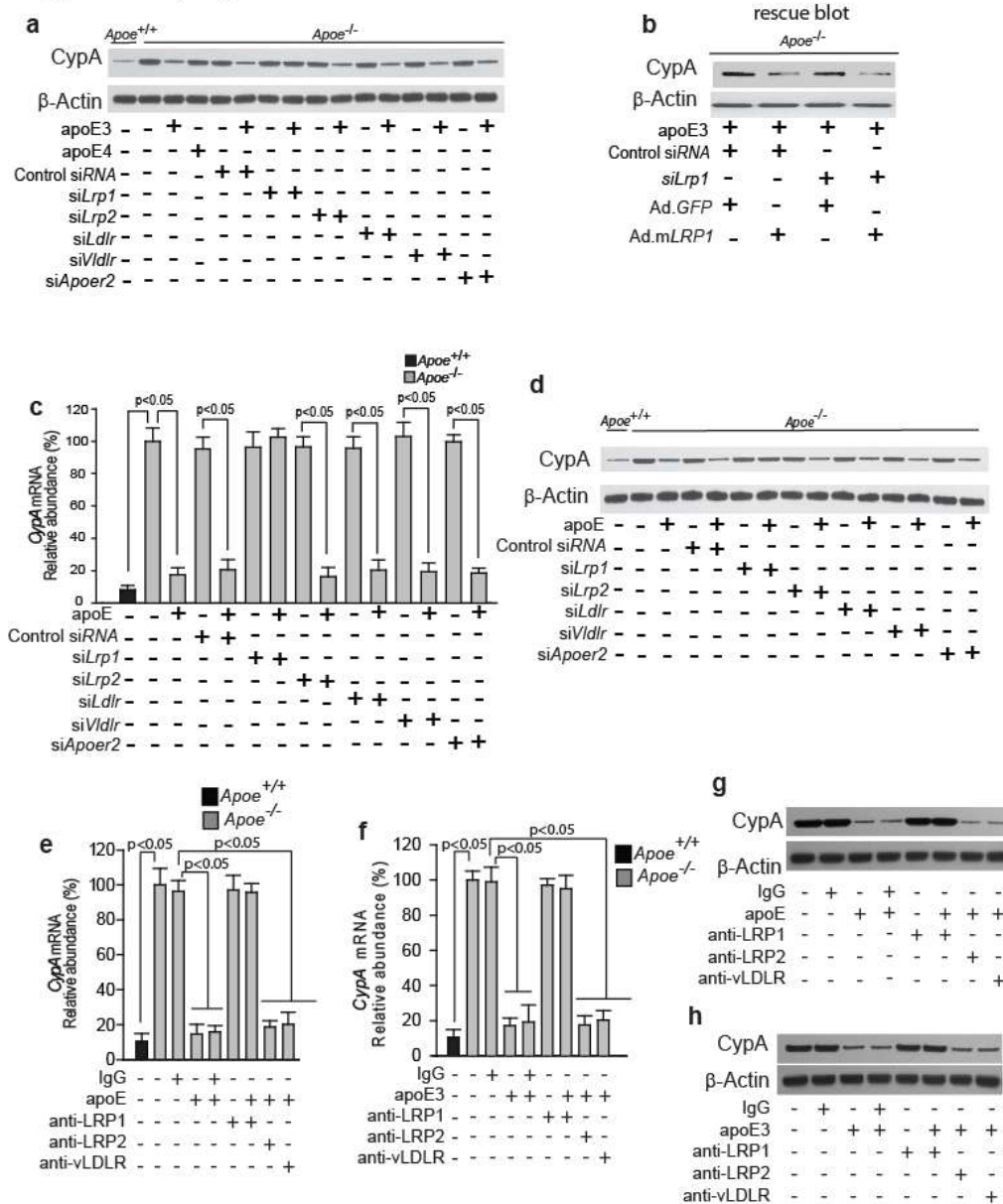
Supplementary Figure 6. Loss of pericyte coverage and microvascular length reductions in *Apoe*^{-/-} and *APOE4* transgenic mice. (a) TUNEL staining (green) in CD13-positive pericytes (red) and lectin-positive capillaries in the cortex of 4-month-old *Apoe*^{+/+} *Ppia*^{+/+}, *Apoe*^{-/-} *Ppia*^{+/+}, *Apoe*^{-/-} *Ppia*^{-/-}, GFAP-APOE3, GFAP-APOE4 and GFAP-APOE4 treated with cyclosporine A. Arrow, TUNEL-positive pericyte. Asterisks, TUNEL-positive endothelial cell. (b) Confocal microscopy analysis of platelet-derived growth factor receptor beta (PDGFRβ)-positive pericyte coverage of lectin-positive capillary profiles in the cortex of *Apoe*^{+/+}, *Apoe*^{-/-}, GFAP-APOE3 and GFAP-APOE4 mice. Scale bar = 25 μm. (c) Quantification of PDGFRβ-positive pericyte coverage of lectin-positive capillary profiles in the cortex and hippocampus of 9 to 12-month-old *Apoe*^{+/+}*Ppia*^{+/+}, *Apoe*^{-/-}*Ppia*^{+/+}, GFAP-APOE3, GFAP-APOE4, TR-APOE3, TR-APOE4 and *Apoe*^{-/-}*Ppia*^{-/-} mice and in TR-APOE4 transgenic mice treated with cyclosporine A, SB-3CT or PDTCT. (d) Confocal microscopy analysis of CD31-positive positive capillary profiles in the cortex of *Apoe*^{+/+} *Ppia*^{+/+}, *Apoe*^{-/-} *Ppia*^{+/+}, *Apoe*^{-/-} *Ppia*^{-/-}, GFAP-APOE2, GFAP-APOE3 and GFAP-APOE4 mice. Scale bar = 25 μm. (e) Negative correlation between capillary length and degree of BBB breakdown causing fibrin accumulation. n=28 mice; r=Pearson's coefficient. In c, mean ± s.e.m., n = 6 animals per group. In a,b and d, representative images of 6 animals per group were shown.

Supplementary Figure 7



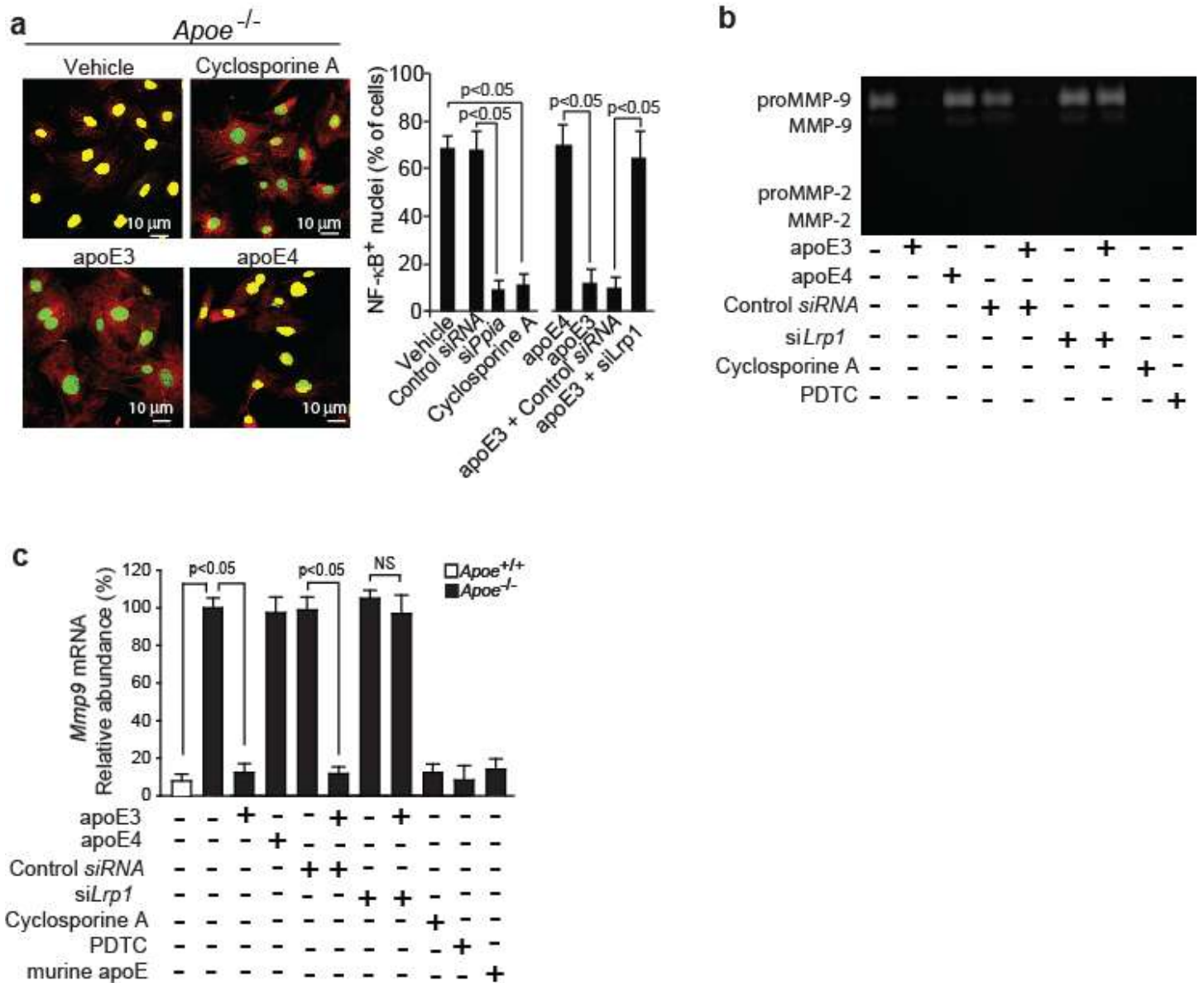
Supplementary Figure 7. LDL/apoE receptor siRNA knockdown validation. (a-e) Immunoblotting analysis of LRP1 (a), LRP2 (b), LDLR (c), vLDLR (d) and APOER2 (e) after treating *Apoe*^{-/-} pericytes with either control siRNA, siLrp1 (a), siLrp2 (b), siLdlr(c), siVldlr (d) or siApoer2 (e). Blots are representative images from 3 independent experiments.

Supplementary Figure 8



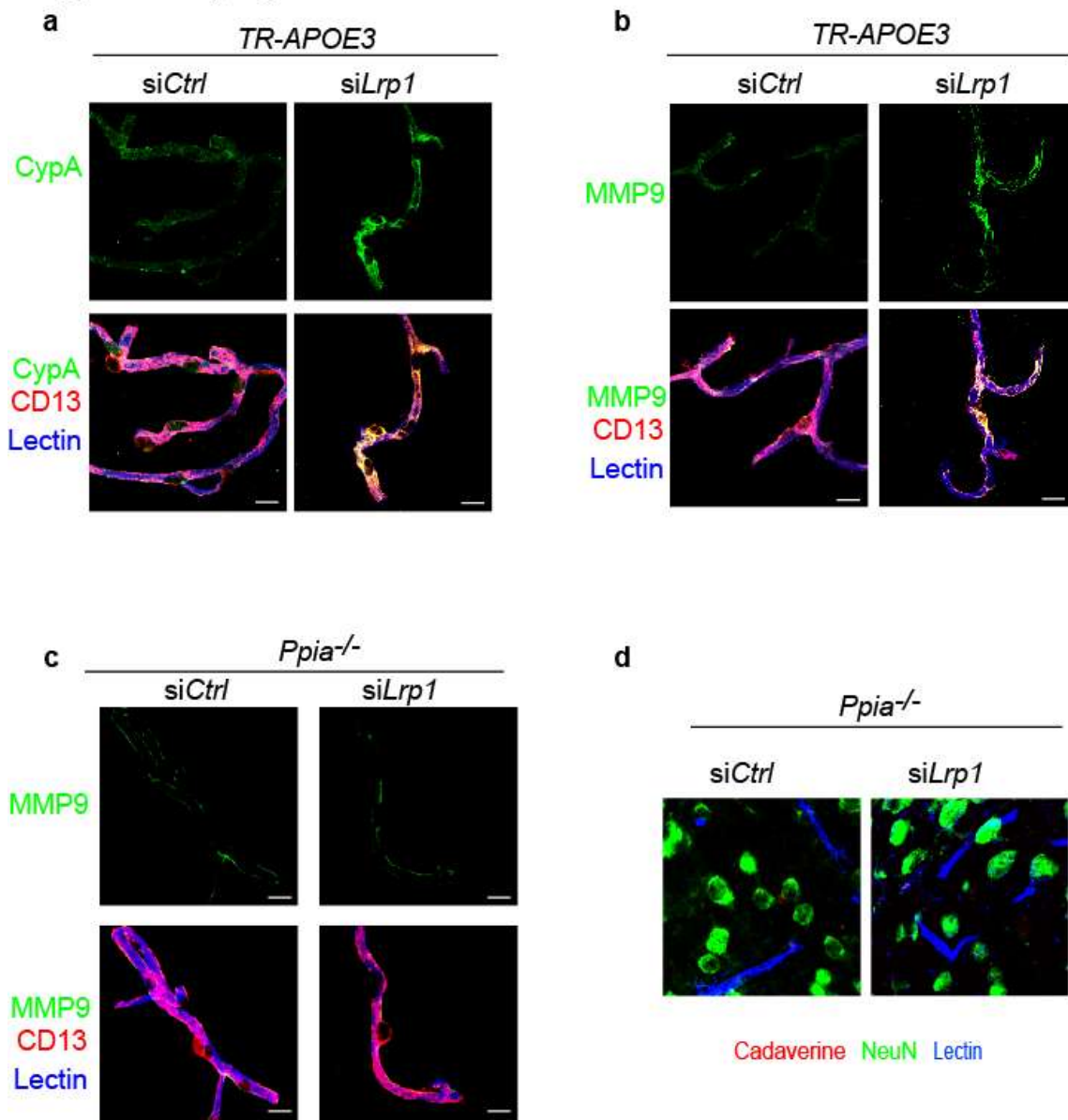
Supplementary Figure 8. ApoE regulates CypA levels via LRP1 in pericytes. (a) CypA protein analysis in *ApoE*^{-/-} pericytes treated with or without 40 nM apoE3 after pre-incubation with vehicle (phosphate-buffered saline), control siRNA or siRNAs targeting the LDL/apoE receptors (siLrp1, siLrp2, siLdlr, siVldlr and siApoer2). (b) Rescue experiment showing CypA protein analysis in *ApoE*^{-/-} pericytes treated with 40 nM apoE3 after control siRNA or siLrp1 treatment subsequent to overexpression of either GFP control (Ad.GFP) or LRP1 minigene (Ad.mLRP1). (c-d) CypA mRNA (c) and protein (d) analysis in *ApoE*^{-/-} pericytes treated with or without 40 nM murine apoE after pre-incubation with vehicle (phosphate-buffered saline), control siRNA or siRNAs targeting the LDL/apoE receptors (siLrp1, siLrp2, siLdlr, siVldlr and siApoer2). (e-h) CypA mRNA (e-f) and protein (g-h) analysis in *ApoE*^{-/-} pericytes 48 h after treatment with mouse apoE or human apoE3 after pre-incubation with vehicle, anti-LRP1, anti-LRP2, anti-vLDLR or non-immune IgG. In a, c and e mean ± s.e.m., n = 3 independent cultures; CypA mRNA abundance in *ApoE*^{-/-} pericytes was arbitrarily set as 100%; the black bar shows levels of CypA mRNA in untreated *ApoE*^{+/+} cells.

Supplementary Figure 9



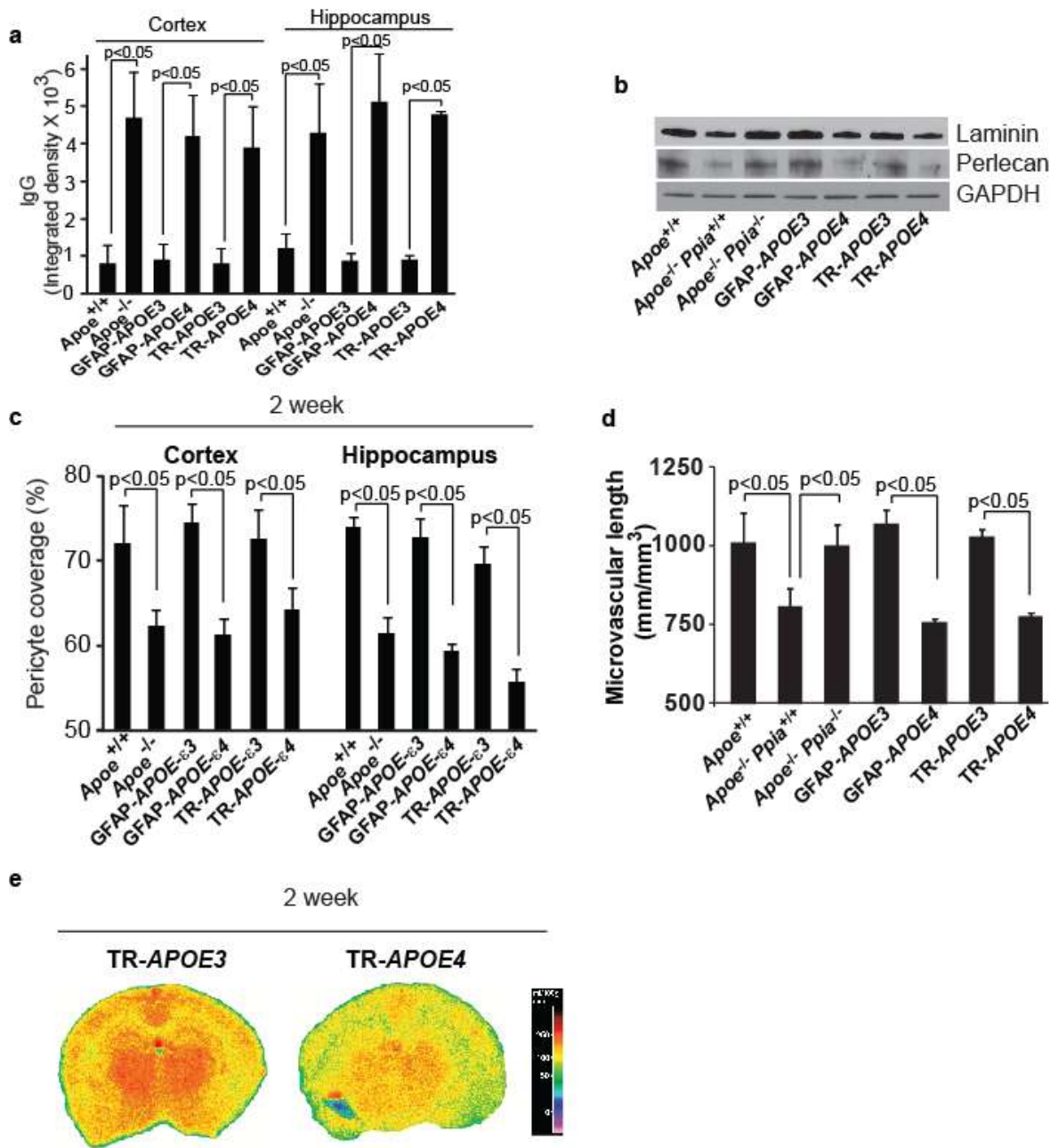
Supplementary Figure 9. ApoE isoform-specific regulation of NF-κB and MMP-9 in pericytes. (a-b) NF-κB nuclear translocation in pericytes (a) and MMP-9 activity in the medium (b) with and without apoE3, apoE4, cyclosporine A, CypA and LRP1 silencing, and PDTC. In a, mean ± s.e.m., n=5-6 animals per group; b, representative results from 6 experiments. (c) Quantification of *Mmp9* mRNA levels by QPCR analysis in *ApoE*^{-/-} pericytes 48 h after treatment with or without astrocytes-derived apoE3, apoE4, apoE3 in the presence of vehicle, control siRNA, siLrp1, cyclosporine A, or PDTC, and murine apoE. Mean ± s.e.m., n=3 independent cultures. The white bar shows levels of *Mmp9* mRNA in untreated *ApoE*^{+/+} cells.

Supplementary Figure 10



Supplementary Figure 10. *In vivo* LRP1 knockdown in TR-APOE3 mice leads to increased CypA and-MMP-9 expression in pericytes and BBB disruption. (a) Confocal images showing CypA colocalization with CD13-positive pericytes on lectin-positive endothelium of TR-APOE3 hippocampal microvessels 72 hours after siLRP1 infusion compared to background CypA levels in mice treated with control siRNA (siCTRL) (b-c) Confocal images of MMP-9, CD13-positive pericytes and lectin-positive endothelium of TR-APOE3 (b) and Ppia^{-/-} (c) hippocampal microvessels 72 hours after control siRNA or siLRP1 infusion. (d) Absence of neuronal uptake (NeuN, green) of cadaverine-Alexa-Fluor-555 (red; yellow, merged) in 6-month-old Ppia^{-/-} mice 72 hours after control siRNA or siLRP1 infusion. Blue, lectin-positive capillaries. In a-c, scale bar = 10 μm, representative results from 3 experiments.

Supplementary Figure 11

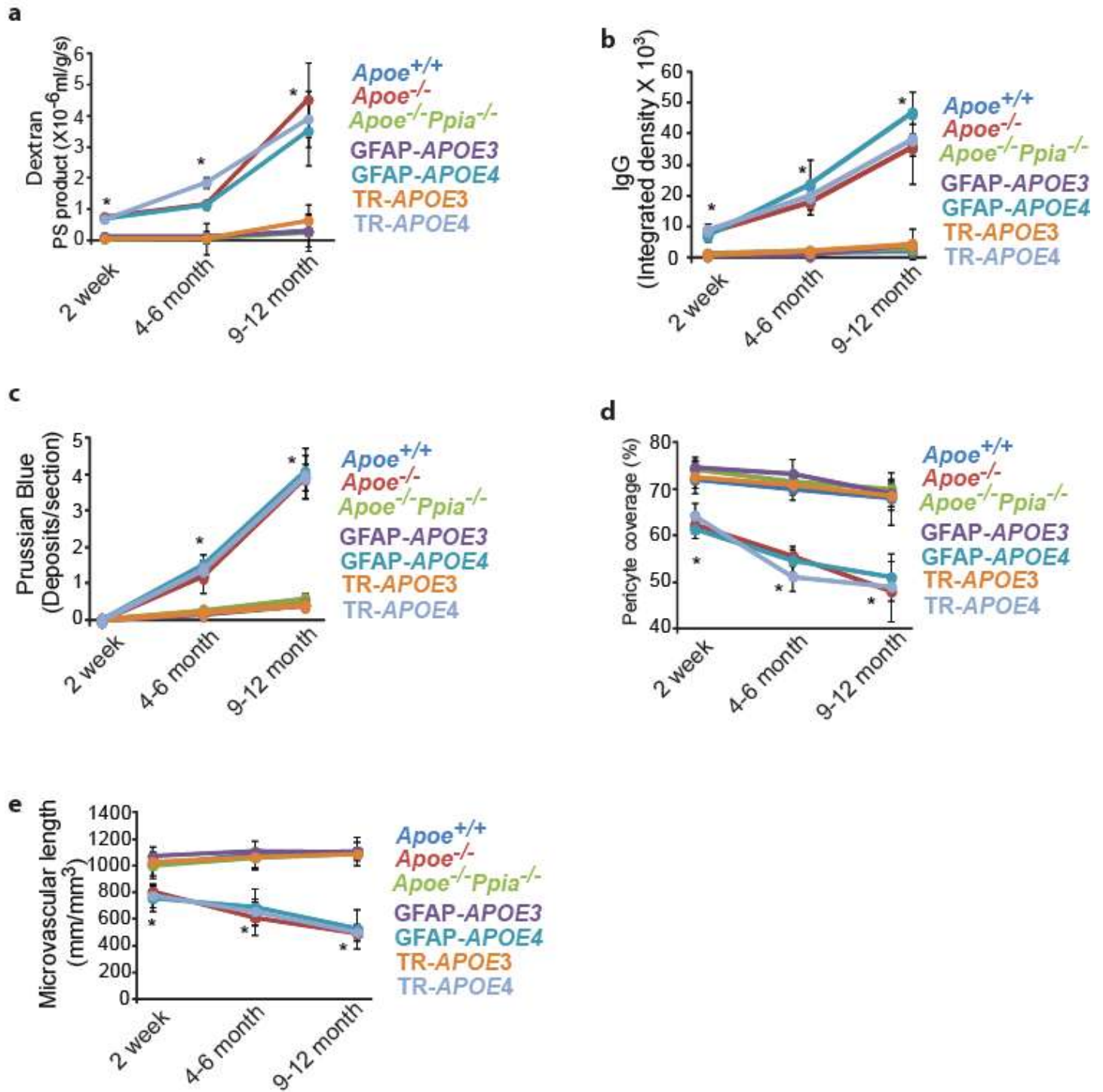


Supplementary Figure 11. Early vascular defects in 2-week old *ApoE*^{-/-} and *APOE4* transgenic mice.

(a) Quantification of extravascular IgG deposits in the cortex and hippocampus of 2-week-old *ApoE*^{+/+}, *ApoE*^{-/-}, GFAP-APOE3, GFAP-APOE4, TR-APOE3 and TR-APOE4 mice. Mean ± s.e.m., n= 5 animals per group.

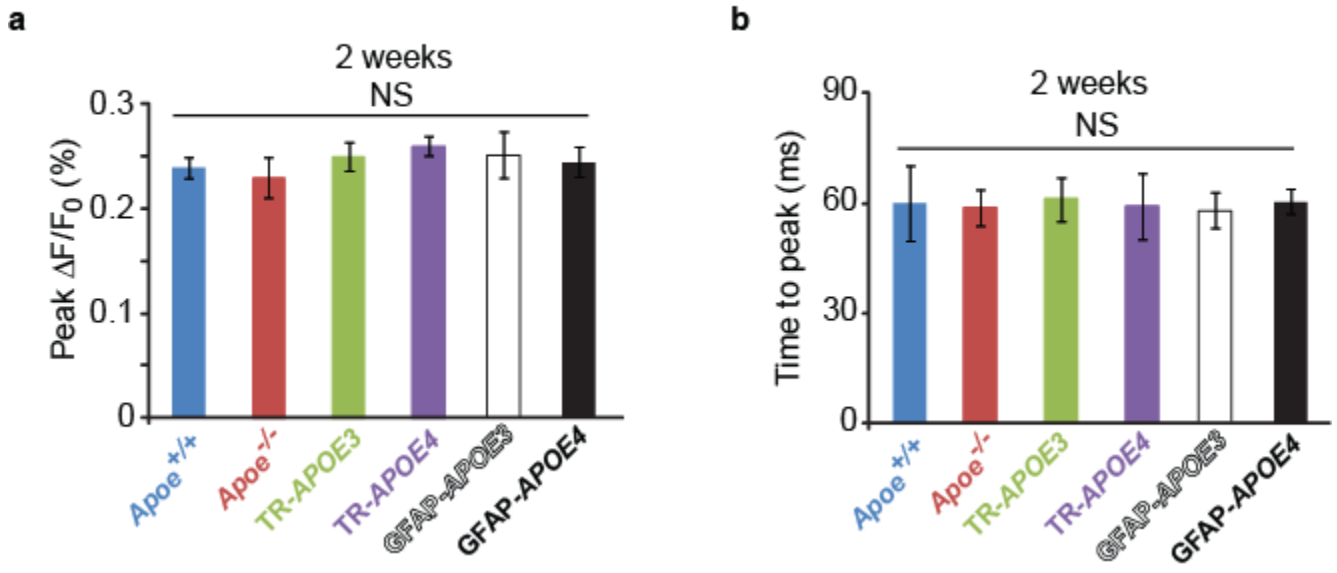
(b) Basement membrane proteins laminin and perlecan and GAPDH in 2 week-old *ApoE*^{+/+}*Ppia*^{+/+}, *ApoE*^{-/-}*Ppia*^{+/+}, *ApoE*^{-/-}*Ppia*^{-/-}, GFAP-APOE3, GFAP-APOE4, TR-APOE3 and TR-APOE4 mice. (c) Quantification of PDGFRβ-positive pericyte coverage of lectin-positive capillary profiles in the cortex of 2-week-old *ApoE*^{+/+}*Ppia*^{+/+}, *ApoE*^{-/-}*Ppia*^{+/+}, GFAP-APOE-ε3, GFAP-APOE-ε4, TR-APOE-ε3 and TR-APOE-ε4 mice. (d) Quantification of the microvascular length in the cortex of 2-week-old *ApoE*^{+/+}*Ppia*^{+/+}, *ApoE*^{-/-}*Ppia*^{+/+}, GFAP-APOE-ε3, GFAP-APOE-ε4, TR-APOE-ε3 and TR-APOE-ε4 mice. (e) Iodoantipyrine autoradiography of CBF in 2-week-old TR-APOE-ε3 and TR-APOE-ε4 mice. In a and c, mean ± s.e.m., n=4-5 animals per group.

Supplementary Figure 12



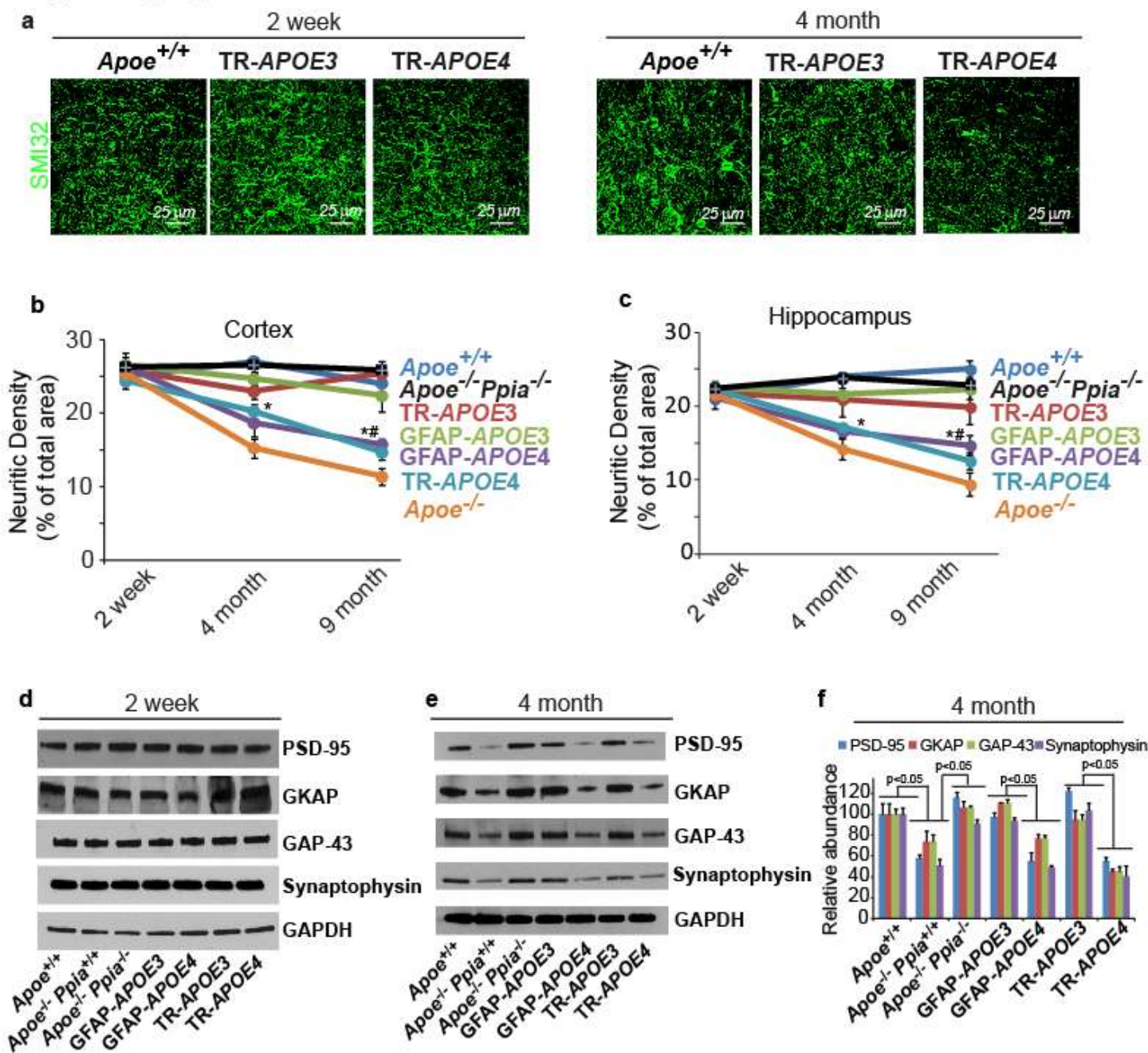
Supplementary Figure 12. Age-dependent pathologic vascular changes in *Apoe*^{-/-} and *APOE4* transgenic mice. (a-e) Quantification of 40 kDa TMR-dextran permeability surface product (PS) (a), extravascular IgG accumulation (b), hemosiderin deposition (c), pericyte coverage (d) and microvascular length (e) in 2-week, 4-6 month and 9-12-month-old *Apoe*^{+/+}, *Apoe*^{-/-}, *Apoe*^{-/-}*Ppia*^{-/-}, GFAP-APOE3, GFAP-APOE4, TR-APOE3 and TR-APOE4 mice. In a-e, mean \pm s.e.m., n=4-5 animals per group.

Supplementary Figure 13



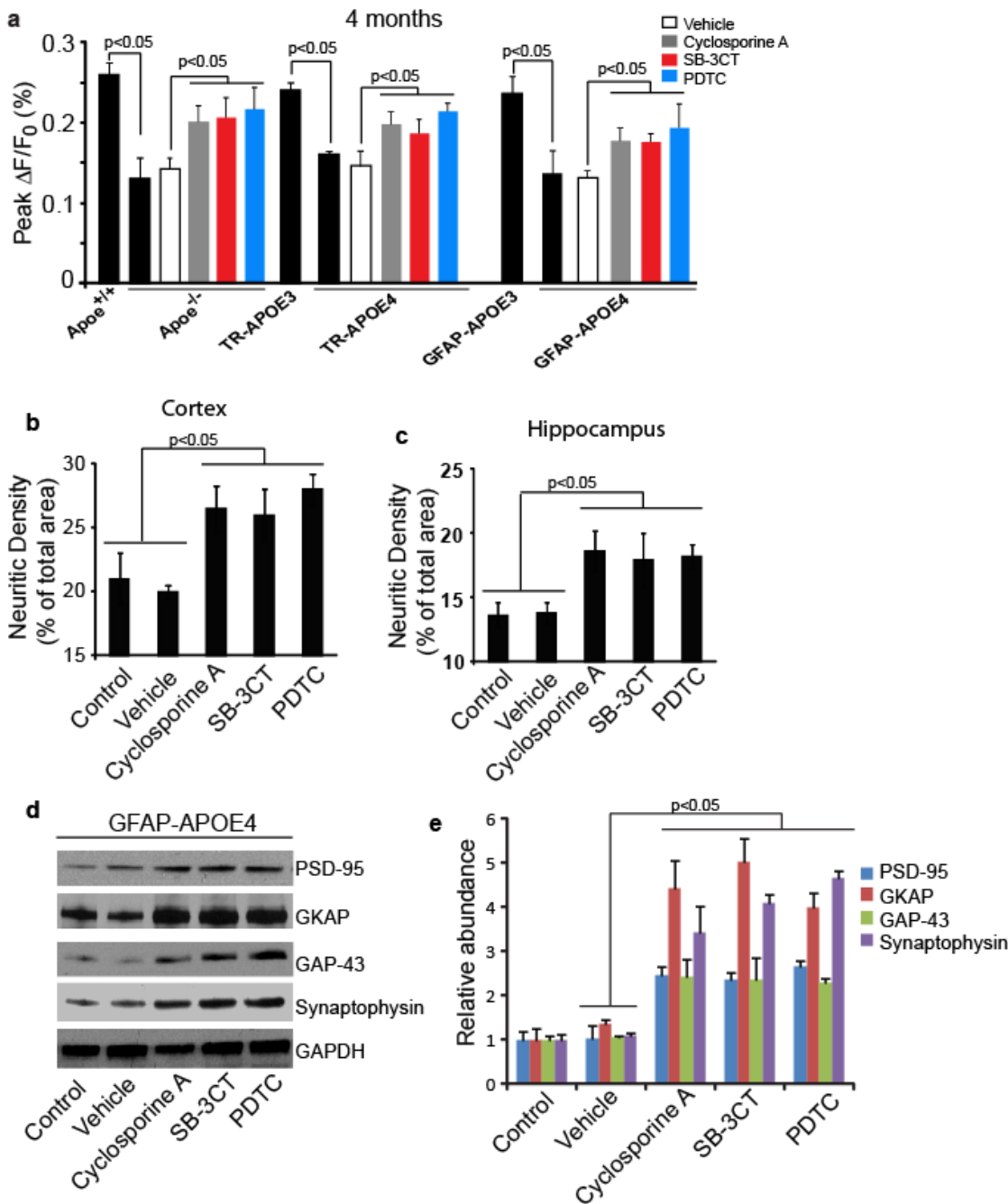
Supplementary Figure 13. Normal sensory evoked neuronal functioning in young *Apoe*^{-/-} and *APOE4* transgenic mice. (a-b) Time to peak fluorescent voltage sensitive dye (VSD) signal (a) and peak change in fluorescent VSD signal (b) in the somatosensory cortex after hind limb stimulation in 2-week-old *Apoe*^{+/+}, *Apoe*^{-/-}, TR-APOE3, TR-APOE4, GFAP-APOE3 and GFAP-APOE4 mice. In a and b, mean \pm s.e.m., n=4-6 animals per group.

Supplementary Figure 14



Supplementary Figure 14. Neuritic density and synaptic proteins in aged *Apoe*^{-/-} and *APOE4* transgenic mice. (a) Confocal microscopy analysis of SMI-32-positive cortical neuritic density (green) in 2-week and 4-month-old *Apoe*^{+/+}, TR-*APOE3* and TR-*APOE4* mice. Scale bar= 20μm. (b-c) Quantification of SMI-32 positive neuritic density in the cortex (b) and hippocampus (c) of 2-week, 4-month and 9-month-old *Apoe*^{+/+}*Ppia*^{+/+}, *Apoe*^{-/-}*Ppia*^{+/+}, *Apoe*^{-/-}*Ppia*^{-/-}, GFAP-*APOE3*, GFAP-*APOE4*, TR-*APOE3* and TR-*APOE4* mice. (d-e) Immunoblot analysis of the pre- and post-synaptic proteins synaptophysin, GAP-43, PSD-95, Shank1 and GKAP normalized to GAPDH in the cortex of 2 week-old (d) and 4 month old (e) *Apoe*^{+/+}*Ppia*^{+/+}, *Apoe*^{-/-}*Ppia*^{+/+}, *Apoe*^{-/-}*Ppia*^{-/-}, GFAP-*APOE3*, GFAP-*APOE4*, TR-*APOE3* and TR-*APOE4* mice. (f) Relative abundance of synaptic proteins in 2-week and 4 month old apoE transgenic mice as in d and e. In b, c and f mean ± s.e.m., n=4-6 animals per group. *p<0.05 when comparing *APOE4* versus *APOE3* mice from the same age group. #p<0.05 when comparing GFAP-*APOE4* to *Apoe*^{-/-} mice from the same age group.

Supplementary Figure 15



Supplementary Figure 15. Chemical blockers of the CypA-NF- κ B-MMP-9 pathway at the BBB improve neuronal and synaptic function and structure in *ApoE*^{-/-} and *APOE4* mice. (a) Peak change in fluorescent VSD signal after hind limb stimulation in 4-month-old *ApoE*^{+/+}, *ApoE*^{-/-}, TR-APOE3, TR-APOE4, GFAP-APOE3 and GFAP-APOE4 mice and in *ApoE*^{-/-}, TR-APOE4 and GFAP-APOE4 mice treated with cyclosporine A, SB-3CT, PDTC or vehicle. Mean \pm s.e.m., n= 5 animals per group. (b-c) Quantification of SMI-32 positive neuritic density in the cortex (b) and hippocampus (c) of 4-month-old *ApoE*^{-/-} and GFAP-APOE4 mice treated with either vehicle, cyclosporine A, SB-3CT or PDTC. (d) Relative abundance of pre- and post-synaptic proteins synaptophysin, GAP-43, PSD-95, Shank1 and GKAP normalized to GAPDH in the cortex of 4-month-old *ApoE*^{-/-} and GFAP-APOE4 mice treated with either vehicle, cyclosporine A, SB-3CT or PDTC. (e) Quantification of the relative abundance of pre- and post-synaptic proteins synaptophysin, GAP-43, PSD-95, Shank1 and GKAP normalized to GAPDH in the cortex of 4-month-old *ApoE*^{-/-} and GFAP-APOE4 mice treated with either vehicle, cyclosporine A, SB-3CT or PDTC. In b, c and e, mean \pm s.e.m., n=4 animals per group.

Table S.1 Regional cerebral blood flow determined by ¹⁴C-iodoantipyrine autoradiography.

All values are mean ± s.e.m., n = 3-5 mice per group. Statistical significance was calculated by one-way ANOVA with Tukey posthoc test and indicated as ^a*P* < 0.05, for *Apoε^{-/-}Ppia^{+/+}* mice vs. *Apoε^{+/-}Ppia^{+/+}* mice or for the TR-*APOE* 4 mice vs. *Apoε^{+/-}Ppia^{+/+}* mice; ^b*P* < 0.05, for the 2-week-old TR-*APOE* 4 mice vs. TR-*APOE* 3 mice.

Regions	<i>Apo^{+/-}Ppia^{+/-}</i> 9 months old	<i>Apoε^{-/-}Ppia^{+/-}</i> 9 months old	<i>Apoε^{+/-}Ppia^{-/-}</i> 9 months old	TR- <i>APOE</i> 2 9 months old	TR- <i>APOE</i> 3 9 months old	TR- <i>APOE</i> 4 9 months old	TR- <i>APOE</i> 3 2 weeks old	TR- <i>APOE</i> 4 2 weeks old
Cerebral Cortex								
Sensorimotor	113.78 ± 9.23	66.88 ± 6.31 ^a	112.21 ± 11.1	119.10 ± 3.52	111.65 ± 6.8	71.77 ± 5.76 ^a	118.92 ± 2.33	88.67 ± 1.98 ^b
Ectorhinal	117.59 ± 7.55	69.72 ± 3.45 ^a	115.55 ± 9.51	121.88 ± 5.17	119.60 ± 2.0	74.27 ± 2.90 ^a	123.64 ± 1.79	92.39 ± 2.65 ^b
Hippocampus	112.22 ± 4.29	62.18 ± 4.81 ^a	107.11 ± 6.84	115.42 ± 6.23	113.41 ± 4.7	67.32 ± 3.00 ^a	121.99 ± 1.81	93.65 ± 2.44 ^b
Caudate-putamen	129.11 ± 8.84	71.46 ± 5.34 ^a	119.56 ± 5.77	124.33 ± 2.22	121.87 ± 3.1	78.00 ± 2.10 ^a	126.44 ± 4.54	92.93 ± 1.39 ^b
Corpus callosum	59.98 ± 4.6	41.31 ± 9.15 ^a	61.22 ± 6.73	61.11 ± 3.21	55.2 ± 4.1	45.11 ± 4.11 ^a	61.46 ± 3.77	48.79 ± 2.34 ^b
Thalamus	162.34 ± 11.15	115.88 ± 7.92 ^a	157.38 ± 5.99	167.21 ± 4.66	159.88 ± 6.0	127.33 ± 6.33 ^a	166.10 ± 4.98	134.2 ± 4.67 ^b

SUPPLEMENTARY MATERIALS AND METHODS

Animals

Mice were housed in plastic cages on a 12 h light cycle with ad libitum access to water and a standard laboratory diet. All studies were performed in accordance with the University of Rochester Institutional Animal Care and Use Committee using National Institute of Health guidelines. All mouse lines were maintained on a C57Bl6 background. *Apoe*^{-/-} mice³¹, GFAP-*APOE* mice on murine apoE null background³², and *Ppia*^{-/-} mice³³ were acquired from Jackson Laboratories. TR-*APOE* mice were generated as previously described¹⁶. The *Ppia*^{-/-} mice were crossed to the *Apoe*^{-/-} and TR-*APOE4* mice to generate the *Apoe*^{-/-}*Ppia*^{-/-} and TR-*APOE4 Ppia*^{-/-} mice used in the present study.

In some studies *APOE4* and *Apoe*^{-/-} mice were treated daily with an intraperitoneal (i.p.) injection of cyclosporine A (Sigma, 30024-25) dissolved in an 80% corn oil 20% ethanol emulsion for 7 consecutive days. The animals were treated with 10 mg/kg on the first 3 days followed by 5 mg/kg/day for the remaining 4 days. This low dose paradigm was utilized because it was previously shown to not cause any systemic or central nervous system toxicity³⁴. In separate studies, *APOE4* and *Apoe*^{-/-} mice were treated with either pyrrolidine dithiocarbamate (PDTC, 100 mg/kg/day) dissolved in saline or SB-3CT (25 mg/kg/day) dissolved in 10% DMSO/50% propylene glycol/40% PBS for seven days.

Blood-brain barrier permeability assays

In vivo multiphoton microscopy analysis

Open-skull glass cover-slipped cranial windows were created as we previously described with some modifications^{14,35}. In brief, mice were anesthetized with an i.p. injection of 750 mg/kg urethane and 50 mg/kg chloralose and the cranium was firmly secured in a stereotaxic frame. A high-speed dental drill (Hager & Meisinger tip) was then used to create a square cranial window about 2 X 2 mm over the parietal cortex, and 45 degree forceps were used to remove the square piece of skull. A sterile 5 mm glass cover slip was then placed above the dura mater and sealed with a 1:1 mixture of bone cement and cyanoacrylate based glue.

Cerebrovascular permeability to dextran

Cortical cerebrovascular permeability was determined using rapid *in vivo* multiphoton microscopy imaging as we previously described^{14,35}. In brief, medium sized TMR-conjugated dextran (40,000 Da, Invitrogen, 0.1 mL of 10 mg/ml) was injected via the left femoral vein. *In vivo* time-lapse images were acquired every 2 min for a total of 30 min. All images were subjected to threshold processing and the extravascular fluorescent intensity was measured using the NIH Image J Integrated Density measurement function by a blinded investigator. The *in vivo* BBB permeability for TMR-dextran was estimated as the PS product as we previously described¹⁴ using the following formula:

$$PS = (1-Hct) 1/I_v \times V \times dI_t/dt$$

Where *Hct* is the hematocrit (45%), *I_v* is the initial fluorescence intensity of the region of interest (ROI) within the vessel, *I_t* is the intensity of the ROI within the brain at time *t*, *V* is the vessel volume, and assuming 1 gram of brain is equivalent to 50 cm².

Cadaverine uptake

Alexa fluor 555-conjugated cadaverine (Invitrogen, A30677) was injected into the tail vein (500 µg/20 gr) and allowed to circulate for 2 h, as previously described¹⁵. For detection and cellular uptake analysis of Alexa fluor 555-conjugated cadaverine, anaesthetized animals were perfused for 1-2 min with HBSS, followed by 5 min perfusion with 4% PFA in PBS. Brains were removed and the tissue was post-fixed in 4% PFA in PBS at 4 °C for 6 h. Forty-µm-thick coronal brain sections were immunostained with mouse anti-NeuN (Millipore, MAB377, 1:250) using the M.O.M. Kit (Vector Laboratories) and stained with fluorescein-conjugated tomato-

lectin overnight in PBS at 4°C to visualize neurons and microvessels, respectively. Sections were then incubated with Dylight 649-conjugated streptavidin (Vector Laboratories, SA-5649, 1:1000) to detect NeuN. After washing with PBS, the sections were coverslipped with fluorescent mounting medium (Dako). The images were pseudo-colored using Zen Software (Zeiss Microimaging Inc.) to better visualize Alexa fluor 555-conjugated cadaverine uptake in NeuN-positive neurons.

Endogenous IgG and fibrin deposits

Mouse endogenous IgG and fibrin was detected as we previously described¹⁴. Mice were anesthetized as described above and transcardially perfused with phosphate buffer saline (PBS) containing 5 U/ml heparin. Brains were removed and embedded into O.C.T. compound (Tissue-Tek) on dry ice, cryosectioned at a thickness of 14-18 µm, and then fixed in acetone. Sections were subsequently blocked with 5% normal swine serum (Vector Laboratories) for 1 h and incubated in the following primary antibodies diluted in blocking solution overnight at 4°C: goat anti-PDGFRβ (R&D, AF1042, 1:200), mouse anti-NeuN (Millipore, MAB377, 1:250) using the M.O.M. kit (Vector Laboratories), goat anti-Thrombin (Santa Cruz Biotechnology, sc-23355, 1:100), rabbit anti-fibrin (Dako, A0080, 1:1000). To visualize immunofluorescent signal the following fluorophore-conjugated secondary antibodies were: Cy3-conjugated bovine anti-goat (Jackson ImmunoResearch, 805-165-180, 1:100) to detect PDGFRβ, Dylight-649-conjugated streptavidin (Vector Laboratories, SA-5649, 1:100) to detect NeuN, Alexa fluor 488-conjugated donkey anti-goat IgG (Invitrogen, A-11055, 1:100) to detect Thrombin and/or Alexa fluor 546-conjugated donkey anti-rabbit (Invitrogen, A10040, 1:200) to detect fibrin. For endogenous IgG detection the sections were first incubated for 48 h with Cy3-conjugated donkey anti-mouse IgG in PBS at 4°C. To visualize brain microvessels, sections were incubated with fluorescein-conjugated tomato lectin (Vector Laboratories FL-1171, 1:200) or biotinylated tomato-lectin (Vector Laboratories, B-1175, 1:1000) followed by incubation with Dylight 649-conjugated streptavidin (Vector Laboratories, SA-5649, 1:1000). Sections were coverslipped using fluorescent mounting medium (Dako) and scanned using a Zeiss 510 meta confocal microscope as described below (please see **Confocal Microscopy Analysis**). Z-stack projections and pseudo-coloring was performed using ZEN software (Carl Zeiss Microimaging).

To quantify extravascular accumulations, the IgG- or fibrin-positive immunofluorescent signals were subjected to threshold processing and measured using the NIH Image J software Integrated Density analysis measurement tool, as we reported¹⁴. We analyzed 6 randomly selected fields from the cortex and 4 randomly selected fields from the hippocampus in 6 non-adjacent sections (~100 µm apart) with at least 4 animals per group.

Prussian blue staining

Mice were anesthetized with urethane (750 mg/kg, i.p.) and chloralose (50 mg/kg, i.p.), then transcardially perfused as described above. Brains were dissected, embedded into O.C.T. compound (Tissue-Tek), cryosectioned at a thickness of 14 µm and fixed in acetone. Sections were incubated in a 5% potassium ferrocyanide and 5% hydrochloric acid solution (1:1 working solution) for 30 min. The sections were then washed with double distilled water and subsequently counterstained with nuclear fast red. Hemosiderin shows blue, whereas the nuclei show red and the cytoplasm shows pink. Six nonadjacent sections (> 100 µm apart) were examined in each mouse. The total number of hemosiderin-positive spots was determined in the cortex and hippocampus. In an earlier short-term study radio-labeled erythrocytes were shown not to leak into the brain within a 1 h time course in *Apoe*^{-/-} mice¹¹. However, our studies on steady-state hemosiderin deposits suggests that erythrocytes do permeate the disrupted BBB in *Apoe*^{-/-} and *APOE4*-expressing mice over time thereby implying that a period of 1 h maybe too short of a time period to detect erythrocyte extravasations.

Non-invasive TMR-Dextran fluorescence spectroscopy

In a separate set of experiments, BBB permeability was assessed using non-invasive fluorescence spectroscopy as we have previously reported¹⁴. In brief, TMR-conjugated dextran (40,000 Da, Invitrogen, 0.1 mL of 10 mg/ml) was injected intravenously via the femoral vein and blood was sampled (20 µL) from the orbital sinus at

2, 10 15, 20 and 30 min in heparanized capillary tubes. Plasma samples were obtained by centrifugation. At the end of the 30 min time period, the animals were transcidentally perfused with PBS containing 5U/ml heparin for 3 min to remove circulating dextran confined in the cerebrovasculature, and the cortex and hippocampus were dissected separately. The tissues were weighed and homogenized in 10 volumes of 1% Triton X-100. All samples were kept on ice, until required for analysis. Next 100 μ l of plasma (diluted 1:20 in 1% Triton X-100) and brain homogenate samples (neat) were then analyzed with a fluorometric plate reader (Victor) using 543 nm excitation and 590 nm emission. The BBB PS product (ml/g/min) was calculated using the following equation as we described¹⁴:

$$PS = Cb / (0 \int TCp \times T)$$

Where Cb and $0 \int TCp$ are the fluorescent tracer concentration in brain (per g) and integrated plasma concentration (per ml), respectively, and T is experimental time.

Isolation of capillaries and microvessel-depleted brain samples

Capillaries were isolated using dextran gradient centrifugation followed by sequential cell-strainer filtrations as we have previously described³⁶. First, mouse brain was carefully isolated and the meninges were removed in ice-cold PBS containing 2% fetal bovine serum (FBS). The cortex and hippocampus were macroscopically dissected and all visible white matter was discarded. The cortex and hippocampus was then minced using a stainless steel razor blade and the brain was homogenized in PBS containing 2% FBS with a glass-douce homogenizer. Dextran (70 kDa, Sigma) was subsequently added to yield a final concentration of 16% and the samples were thoroughly mixed. The samples were then centrifuged at 6,000 g for 15 min. The microvessel-depleted brain (brain tissue minus capillaries) remained on top of the dextran gradient and was collected. The capillary pellet located at the bottom of the tubes was collected and sequentially filtered through a 100 μ m and 45 μ m cell strainer (BD Falcon). The capillaries remaining on top of the 45 μ m cell strainer were collected in PBS and either lysed for immunoblot analysis, cytospun for fluorescent staining analysis, or processed for establishing primary pericyte cell cultures as described below.

Immunoblotting analysis

Microvessel-depleted brains, isolated brain capillaries and primary mouse brain pericytes were rinsed twice in ice cold PBS and then lysed in RIPA buffer (50 mM Tris, pH 8.0, 150 mM NaCl, 0.1% SDS, 1.0% NP-40, 0.5% sodium deoxycholate and Roche protease inhibitor cocktail). All samples were subjected to SDS-Page gel electrophoresis and transferred to a nitrocellulose membrane. Membranes were blocked with 5% milk, incubated with primary antibodies, and then incubated with the appropriate HRP-conjugated secondary antibody. Membranes were then treated with Immobilon Western ECL detection buffers (Millipore), exposed to CL-XPosure film (Thermo Scientific) and developed in an X-OMAT 3000 RA film processor (Kodak). The following primary antibodies were utilized for immunoblot analysis (antibodies are listed in order of appearance in the manuscript): rabbit anti-CypA (Abcam, ab42408, 1:1000), rabbit anti-GAPDH (Cell Signaling Technology, 2118, 1:5000), goat anti-Thrombin (Santa Cruz Biotechnology, sc-23355, 1:100), goat anti- β Actin (Santa Cruz Biotechnology, sc-1616, 1:1000), rabbit anti-collagen IV (Abcam, ab52235, 1:500), rabbit anti-ZO-1 (Invitrogen, 40-2300, 1:250), Mouse anti-Occludin (BD Biosciences, 16453, 1:100), goat anti-Claudin 5 (BD Biosciences, 17645, 1:100), rabbit anti-RELA (Cell Signaling, 3987, 1:250), rabbit anti-MMP-9 (Abcam, ab38898, 1:500), rabbit anti-MMP2 (Cell Signaling, 4022, 1:1000), goat anti-IgG (Dako, 172-1011, 1:100), mouse anti-LRP1 (Calbiochem, 438192, 1:1000), goat anti-LDLR (R&D Systems, AF2255, 1:500), goat anti-VLDLR (R&D Systems, AF2258, 1:500), mouse anti-LRP2 (Abcam, ab218491:1000) and anti-ApoER2 (Sigma, A3481, 1:1000), rabbit anti-laminin (Sigma, L9393, 1:500), rat anti-perlecan (Santa Cruz Biotechnology, sc-33707, 1:250), rabbit anti-synaptophysin (Cell Signaling, 5461, 1:1000), rabbit anti-GAP-43 (Cell Signaling, 8945, 1:1000), rabbit anti-PSD95 (Cell Signaling, 3450, 1:1000), goat anti-Shank (Santa Cruz Biotechnology, sc-23542, 1:250) and goat anti-GKAP (Santa Cruz Biotechnology, sc-31522, 1:250).

Relative protein abundance

Images were acquired and densitometry analysis was performed using an AlphaImager 2200 and AlphaEase FC software (Alpha Innotech Corporation), respectively. The signal intensity of all protein bands were normalized to the GAPDH or β -actin loading control band.

Immunofluorescent CypA analysis

The area of CypA-positive staining in PDGFR β -positive pericytes was determined using immunofluorescent detection. Brain capillaries were isolated as described above and subsequently cytospun (500 g) for 5 min onto Superfrost Plus pre-cleaned glass microscopy slides. The microvessel fragments were then fixed using ICC Fixation Buffer (BD Pharmingen, 550010) for 15 min at room temperature. The microvessels were then rinsed with PBS and blocked in PBS containing 0.4% Triton X-100 and 5% Swine Serum (Vector Laboratories) for 1 h at room temperature followed by incubation with the following primary antibodies including rabbit anti-CypA (Abcam, ab42408, 1:1000) and goat anti-PDGFR β antibody (R&D, AF1042, 1:200) and with biotin-conjugated tomato lectin (Vector Laboratories) overnight at 4° C. To detect PDGFR β and lectin, sections were incubated with Fluorescein-conjugated donkey anti-rabbit IgG (Jackson ImmunoResearch, 1:100), Cy3-conjugated bovine anti-goat IgG (Jackson ImmunoResearch Laboratories, 805-165-180, 1:500) and Dylight 649-conjugated streptavidin (Vector Laboratories), respectively.

***In vivo* multiphoton imaging of MMP gelatinase activity**

In vivo detection of MMP gelatinase cerebrovascular activity was done as previously described²⁵. Briefly, mice were anesthetized and cranial windows were made as described above. The dura was surgically removed and 20 μ l of DQ-Gelatin (E-12055, Invitrogen) was incubated on brain surface for 20 min. After washing the area with sterile artificial CSF a sterile 5 mm glass cover slip was sealed over the cranial window as described above. Texas-Red-conjugated mega-dextran 2,000,000 Da (0.1mL of 10 mg/ml, D7139) was injected via the tail vein and *in vivo* images were acquired using custom built Zeiss 5MP multiphoton microscope (Carl Zeiss Microimaging). A 900 nm mode locked DeepSee Ti:sapphire laser (Mai Tai, Spectra Physics, Mountain View, CA) was used to excite DQ-Gelatin fluorescent and Texas Red and signal emission was detected through a 500-550 and 650-710 band-pass filter, respectively. The integrated density of the fluorescent signal of DQ-Gelatin was measured using the NIH ImageJ software. In a separate set of experiments animals were treated with i.p. injections of cyclosporine A (5-10 mg/kg/day), pyrrolidine dithiocarbamate (PDTC, 100 mg/kg/day) or SB-3CT (25 mg/kg/day) for seven days before MMP gelatinase was determined.

Brain tissue gelatinase zymography

Animals were anesthetized as described above and transcardially perfused with PBS containing 5U/ml heparin. Next, cortical brain tissue (~50 mg) was manually dissected, homogenized in lysis buffer (50 mM Tris-HCl, pH 7.6, 150 mM NaCl, 5 mM CaCl₂, 0.05% Brij35, 0.02% NaN₃, 1% Triton X-100) and then concentrated using gelatin-sepharose G beads (GE Healthcare). The samples were separated on an 8% polyacrylamide SDS gel containing 1mg/ml gelatin (Sigma, St. Louis, MO). The gel was then soaked in 2.5% Triton X-100 for 30 min at room temperature followed by a 16 h incubation at 37 °C in a buffer containing 50 mM Tris-HCl, pH 8.5, 200 mM NaCl, 5 mM CaCl₂, and 0.02% Brij 35. To visualize the MMPs, the gel was stained with SimplyBlue Safe Stain (Invitrogen) according to the manufacturer's instructions. In a separate set of experiments animals were treated with i.p. injections of cyclosporine A (5-10 mg/kg/day), PDTC (100 mg/kg/day) or SB-3CT (25 mg/kg/day) for seven days before MMP gelatinase activity was measured.

Immunofluorescent MMP-9 analysis

The area of MMP-9-positive staining in CD13-positive pericytes was determined using immunofluorescent detection. Brain capillaries were isolated as described above and subsequently cytopun (500 g) for 5 min onto Superfrost Plus pre-cleaned glass microscopy slides. The microvessel fragments were then fixed using ICC Fixation Buffer (BD Pharmingen, 550010) for 15 min at room temperature. The microvessels were then rinsed with PBS and blocked in PBS containing 0.4% Triton X-100 and 5% Swine Serum (Vector Laboratories) for 1 h at room temperature followed by incubation with the following primary antibodies rabbit anti-MMP-9 (Abcam, ab38898, 1:100) and goat anti-CD13 antibody (R&D, AF2335, 1:100) and with biotin-conjugated tomato lectin (Vector Laboratories) overnight at 4° C. To detect MMP-9, CD13 and lectin, sections were incubated with Fluorescein-conjugated donkey anti-rabbit IgG (Jackson ImmunoResearch, 1:100), Cy3-conjugated bovine anti-goat IgG (Jackson ImmunoResearch Laboratories, 805-165-180, 1:500) and Dylight 649-conjugated streptavidin (Vector Laboratories), respectively. MMP-9-positive area was expressed as a percentage of CD13-positive pericyte area using the Image J Area measurement tool. Approximately 100 vessels were analyzed per animal with a total of 6 animals per group. In a separate set of experiments TR-*APOE4* mice were treated with i.p. injections of cyclosporine A (5-10 mg/kg/day) or PDTC (100 mg/kg/day) for seven days before MMP-9 studies.

Immunofluorescent ZO-1 tight junction analysis

The area of ZO-1-positive tight junctions occupying lectin-positive capillary profiles was determined as we have previously reported¹⁴. Acetone fixed sections were prepared and blocked as described above followed by incubation with mouse anti-ZO-1 (Invitrogen, 33-9100, 1:50) using the M.O.M. kit (Vector Laboratories) and 546-conjugated streptavidin (Vector Laboratories). Lectin staining was then performed as described above. The area of ZO1-positive tight junctions was normalized to the total area of lectin-positive microvessels using the Image J Area measurement tool as we have previously described¹⁴. Six animals per group were analyzed. In a separate set of experiments animals were treated with i.p. injections of cyclosporine A (5-10 mg/kg/day) or SB-3CT (25 mg/kg/day) for seven days before ZO-1 tight junction analysis was determined.

Immunofluorescent collagen IV analysis

The area of collagen IV-positive basement membrane occupying lectin-positive capillary profiles was determined by immunofluorescent detection. Acetone fixed sections were prepared and blocked as described above followed by incubation with rabbit anti-collagen IV (Invitrogen , 64754, 1:1000) and Cy3-conjugated donkey anti-rabbit (Jackson Immunological Research). Lectin staining was then performed as described above. The area of collagen IV-positive basement membrane was normalized to the total area of lectin-positive microvessels using the Image J Area measurement tool as we have previously described¹⁴. Six animals per group were analyzed. In a separate set of experiments animals were treated with i.p. injections of cyclosporine A (5-10 mg/kg/day) or SB-3CT (25 mg/kg/day) for seven days before ZO-1 tight junction analysis was determined.

Microvascular NF-κB immunofluorescent staining

Brain capillaries were isolated as described above and subsequently cytopun (500 g) for 5 min onto Superfrost Plus pre-cleaned glass microscopy slides. The microvessel fragments were then fixed using ICC Fixation Buffer (BD Pharmingen, 550010) for 15 min at room temperature. The microvessels were then rinsed with PBS and blocked in PBS containing 0.4% Triton X-100 and 5% Swine Serum (Vector Laboratories) for 1 h at room temperature. The microvessels were then incubated with rabbit anti-NFκB (Cell Signaling, 6956S, 1:100), goat anti-CD13 (R&D, AF2335, 1:100) and biotinylated tomato-lectin (Vector Laboratories, B-1175, 1:1000) in PBS overnight at 4°C. After washing with PBS, the microvessels were incubated with fluorescein-conjugated donkey anti-rabbit IgG (Jackson ImmunoResearch Laboratories, 711-095-152, 1:500), Cy3-conjugated bovine anti-goat IgG (Jackson ImmunoResearch Laboratories, 805-165-180, 1:500) and Dylight 649-conjugated streptavidin

(Vector Laboratories, SA-5649, 1:1000) for 1 h at room temperature. DAPI nuclear acid stain (Invitrogen) was used to visualize nuclei. The vessel fragments were then washed with PBS and coverslipped with fluorescent mounting medium (Dako). The number of NF- κ B-positive nuclei of CD13-positive pericytes was counted and expressed as a percentage of the total number of nuclei in CD13-positive pericytes. This analysis was performed on one hundred vessels per animal with 6 animals per group total.

In situ fluorescent TUNEL staining

Fluorescent TUNEL staining was performed as we have previously described¹⁴. Paraformaldehyde-fixed, paraffin-embedded brain tissue sections were sectioned at a thickness of 7 μ m. The DeadEnd Fluorometric TUNEL system (Promega) was performed as described by the manufacturer. The sections were then blocked with 10% swine serum (Vector Laboratories) and incubated with goat anti-CD13 antibody (R&D, AF2335, 1:100) and biotin-conjugated tomato lectin (Vector Laboratories) overnight at 4° C. To detect CD13 and lectin, sections were incubated with Cy3-conjugated bovine anti-goat IgG (Jackson ImmunoResearch Laboratories, 805-165-180, 1:500) and Dylight 649-conjugated streptavidin (Vector Laboratories), respectively, for 1 h at room temperature. Sections were cover slipped using fluorescent mounting medium (Dako) in preparation for imaging.

Pericyte coverage analysis

Pericyte coverage analysis was performed as we have previously described^{14, 37}. In brief, PDGFR β or CD13 and lectin staining was performed in acetone fixed tissue sections as described above and signals from microvessels \leq 6 μ m in diameter were separately subjected to threshold processing. The areas occupied by their respective signals were analyzed using the NIH Image J Area measurement tool. Pericyte coverage was quantified as a percentage (%) of PDGFR β -positive pericyte surface area covering lectin-positive capillary surface area per field (420 x 420 μ m). In each animal 6 randomly selected fields from the cortex and 4 randomly selected fields from the hippocampus were analyzed in 6 nonadjacent sections (~100 μ m apart). Four-six animals per group were analyzed as indicated in the figure legends.

Microvascular length measurements

The length of CD31-positive capillary profiles was determined as we have previously reported¹⁴. Acetone fixed tissue sections were prepared and blocked as described above followed by incubation with rat anti-CD31 (BD Pharmingen, 550274, 1:50) and Cy3-conjugated donkey anti-rat (Jackson ImmunoResearch, 712-165-150, 1:100). The capillary profile length (vessels \leq 6 μ m in diameter) was measured using the Image J “Neuro J” plug-in length analysis tool from 6 randomly selected fields in the cortex (420 x 420 μ m) and 4 randomly selected fields in the hippocampus (420 x 420 μ m) per section from 6 non-adjacent (~100 μ m apart) sections per animal, as we described¹⁴. The length was expressed in mm of CD31-positive vascular profiles per mm³ of brain tissue. Six animals per group were analyzed.

Cerebral blood flow autoradiography

Regional CBF was determined by combining intraperitoneal (i.p.) ¹⁴C-IAP tracer application with a single blood sampling from the heart at the end of the experiment, as we and others described^{14, 38}. Briefly, mice anesthetized with 2-3% isoflurane in 30% oxygen and 70% nitrous oxide was injected with ¹⁴C-IAP (15 μ Ci, American Radiolabeled Chemicals, Inc.) in 100 μ l saline. Prior to ¹⁴C-IAP administration, arterial blood pressure was recorded via the cannulated right femoral artery using a pressure transducer (AD instruments). A small sample of blood from the femoral artery (90 μ L) was used to determine arterial pH and blood gases using the Radiometer ABL 77 (Copenhagen). Precisely 30 s after ¹⁴C-IAP injection mice were decapitated and quickly immersed in liquid nitrogen until frozen. Frozen blood from the left ventricle of the heart was carefully removed in a cold room (0 °C) and placed in pre-weighed tubes. Blood samples were decolorized with hydrogen peroxide

to reduce quenching, and analyzed for ^{14}C -IAP radioactivity with a liquid scintillation counter (Tri-Carb[®] 2700 TR, Packard Instrument Company) after dissolving the samples overnight with 0.5 ml aqueous based tissue solubilizer (Solvable[™], PerkinElmer Life and Analytical Sciences) and adding 5 ml high flash-point LSC-cocktail (Ultima Gold[™], PerkinElmer). The frozen brains were carefully removed in the cold room and embedded in O.C.T. medium (Tissue-Tek.) on dry ice. Brains were cryosectioned at 20 μm , mounted on glass slides, dried on a hot plate at 50°C for 10 min and exposed to BioMax MR autoradiographic film (Kodak) along with calibrated autoradiographic ^{14}C standards (GE Healthcare UK Ltd., Little Chalfont). After 2-4 weeks of exposure, the film was developed and resulting images were analyzed with a MCID[™] imaging analyzer (InterFocus Imaging Ltd.) to determine levels of ^{14}C -IAP in different brain regions by quantitative autoradiography.

Regional cerebral blood flow calculations

Blood flow, F (ml/100g/min) through different brain regions was determined as previously described¹⁴ using the following equation:

$$F = \frac{\dot{e}}{T} \ln \left(\frac{1 - C_i(T)}{\dot{e}_0} \right) \int_0^T C_A(T)$$

Where $C_i(T)$ is ^{14}C -IAP radioactivity (d.p.m.)/gram of brain tissue, T is the experimental time in s, $C_A(T)$ is ^{14}C -IAP radioactivity (d.p.m.)/gram plasma determined as ^{14}C -IAP integrated plasma concentration (\int_0^T) from ^{14}C -tracer lag time after ^{14}C -IAP i.p. injection (zero time) to the value measured in the blood sample from the frozen heart at the end of the experiment (at time T), by assuming a linear rise or ramp function over T, and \dot{e} is ^{14}C -IAP central nervous system tissue to blood partition coefficient, 0.8 ml/g. The local blood flow was calculated with the MCID program. Values were mean \pm S.E.M. from 6 mice per group.

Brain pericyte cultures

Primary mouse brain pericytes were isolated for *in vitro* culturing as previously described³⁹. Specifically, isolated microvessel fragments were digested for 12 h at 37°C with collagenase A (Roche, 10103586001), constant shaking and vigorous pipetting every 3-4 h. The cells were then spun down and washed with PBS and then plated in complete medium containing DMEM, 10% FBS, 1% non-essential amino acids, 1% vitamins and 1% antibiotic/antimycotic on plastic (non-coated) tissue culture plates. After 6 to 12 h the non-adherent cells were rinsed away and fresh medium was replaced every 2-3 days. Cultures were confirmed to be morphological consistent with pericyte cultures and PDGFR β -positive, SMA-positive, Desmin-positive, GFAP-negative, AQP4-negative, MAP2-negative, NeuN-negative, VWF-negative, and Iba1-negative (data not shown).

For *in vitro* culture studies, the cells were incubated in complete medium as described above and used up to passage 6. The murine apoE used in these studies was isolated from mouse plasma by affinity column chromatography²⁸ and astrocytes-derived lipidated human apoE3 and apoE4 were prepared and purified from conditioned media of immortalized mouse astrocytes isolated from *APOE3*- and *APOE4*-knock-in mice as described^{28, 40}. ApoE receptor knock down was accomplished utilizing the following siRNA oligonucleotides: si*Lrp1* (Dharmacon, E-040764-00-0010), si*Lrp2* (Dharmacon, E-045961-00-0010), si*Ldlr* (Dharmacon, E-0485752-00-0010), si*Vldlr* (Dharmacon, E-046834-00-0010) and si*Apoer2* (Dharmacon, E-046407-00-0010). All siRNA oligonucleotide pools were transfected into cells using Lipofectamine 2000 (Invitrogen). Control siRNA (Dharmacon) that does not degrade any known mammalian mRNA was also used in these experiments. We also used specific function-blocking antibodies raised against the extracellular domain of LRP1 (Santa Cruz Biotechnology, N20), LRP2 (a generous gift from Dr. Scott Argraves, Medical University of South Carolina) and vLDLR (R&D, AF2258). For instance the LRP1 antibody (N20) has been shown to block binding and endocytosis of LRP1 ligands in brain endothelium or other types of vascular cells *in vitro* and *in vivo* including: Alzheimer's A β , apoE isoforms 2 and 3, tPA, MMP, APP, etc⁴¹⁻⁴⁴, as well as signaling via LRP1 regulating nitric oxide synthase (Zlokovic lab, unpublished observations). It has also been shown that the LRP2 antibody (obtained from Scott Argraves) that we used in the current study blocks binding and clearance of LRP2-specific ligand apoJ by brain endothelial cells and across the BBB *in vivo*^{42, 45}. This same LRP2 antibody has also been

used to specifically block other LRP2 ligands such as Sonic Hedgehog⁴⁶ and Seminal Vesicle Secreted Protein II⁴⁷. The VLDLR antibody used in our studies has been shown to block VLDLR-mediated endocytosis of apoE2, 3 and 4 in brain endothelial cells including lipidated astrocyte-secreted apoE isoforms, as used in the present study, and lipid-free forms of apoE²⁸. Therefore, these 3 antibodies provide important independent evidence complementing the siRNA evidence to deduce whether LRP1, LRP2 and/or VLDLR in pericytes participate or not in signaling mediated by astrocyte-derived apoE isoforms utilized in this experiment.

In a separate set of experiments other known LRP1 ligands besides apoE were tested to see if they elicited an effect on CypA protein expression. In brief, cells were prepared as described above and then treated with 40 nM of either monomeric or oligomeric A β 40 or A β 42 (W. M. Keck Facility, Yale University), RAP (EMD Biosciences), activated (*) a2M (AbD Serotec), aprotinin (Abcam), tPA (Cell Sciences), MMP9 (R&D Systems), Factor IXa (HTI) or sAPP β (a generous gift from Dr. Sam Sisodia).

CypA protein levels were determined by immunoblotting as described above. *Cypa* mRNA levels were determined by isolating total mRNA with the RNeasy Mini kit (Qiagen Inc). The mRNA was then reverse-transcribed to cDNA using the iScript cDNA Synthesis kit (Bio-Rad, Hercules). The following primers were used for amplification: mouse *GAPDH*, sense 5'- GTCATTGAGAGCAATGCCAG -3', anti-sense 5'- GTGTTCCCTACCCCAATGTG-3'; mouse *CypA*, sense 5'- AGCATACAGGTCCTGGCATCTTGT -3', anti-sense 5'-AAACGCTCCATGGCTTCCACAATG -3'. Quantitative PCR was performed using iQ SYBR Green Supermix (Bio-Rad) and IQ4 multicolor detection QPCR system (Bio-Rad). The relative abundance of mouse *Cypa* mRNA was normalized to *Gapdh* mRNA.

Fluorescent *in situ* ApoE/LRP1 proximity ligation assay

Proximity ligation was performed as we have previously reported³⁷ to determine apoE isoform-specific binding to LRP1. In brief *ApoE*^{-/-} pericytes, isolated as described above, were plated on multi-spot glass slides. The cells were incubated with 40 nM of either astrocytes-derived apoE3 or apoE4 for 30 min at 4°C. The cells were subsequently washed in cold PBS, fixed in ice cold 4% paraformaldehyde for 10 min and then blocked with 10% normal swine serum (Vector Laboratories) for 1 h at room temperature. Next the cells were incubated with goat anti-ApoE (Calbiochem, 3D12 1:100) and rabbit anti-LRP1 (Sigma, L2295, 1:100) overnight at 4°C. Proximity ligation was then conducted as described by the manufacturer (Olink Bioscience; Uppsala, SE) utilizing the Duolink II PLA probe anti-goat PLUS, Duolink II PLA probe anti-rabbit MINUS, and Duolink II detection reagents green to visualize the specific ApoE isoform-LRP1 interactions. Cells were then rinsed with PBS and incubated with Alexa 594-conjugated *phalloidin* (Invitrogen, 1:1000) for 30 min at room temperature in order to visualize cellular morphology. To visualize nuclei the cells were incubated with Hoechst (Invitrogen, 1:10,000) for 10 min at room temperature. The slides were then coverslipped using fluorescent mounting medium (Dako) and confocal microscopy imaging was performed as described below (see **Confocal Microscopy Analysis**).

In vitro NF- κ B immunofluorescent detection

ApoE^{-/-} pericytes were isolated and cultured on multi-spot slides as described above. The cells were treated with either vehicle control, control siRNA (Dharmacon, D-001910-10-20), si*Ppia* (Dharmacon, E-040767-00-0010), cyclosporine A (Sigma, 50 ng/ml), astrocytes-derived lipidated apoE4 or apoE3 (40 nM) in the presence of either control siRNA or si*Lrp1* for 48 h. The cells were then rinsed in ice-cold PBS and fixed in 4% paraformaldehyde for 10 min. Next the cells were permeabilized with 0.4% Triton X-100 in PBS for 10 min then blocked for 1 h at room temperature with 10% swine serum in PBS. The cells were then incubated overnight with mouse anti-NF κ B (Cell Signaling, 6956S, 1:100) overnight at 4°C, washed in PBS then incubated with fluorescein conjugated donkey anti-mouse IgG (Jackson Immunological Research, 1:100). To visualize nuclei the cells were incubated with Hoechst (Invitrogen, 1:10,000) for 10 min at room temperature. The slides were then coverslipped using fluorescent mounting medium (Dako) and confocal microscopy imaging was performed as described below (see **Confocal Microscopy Analysis**). NIH image J "Cell Counter"

plugin was utilized to count the number of NF- κ B-and Hoescht-positive nuclei in order to calculate the percentage of NF- κ B positive nuclei.

Confocal microscopy analysis

All coverslipped mounted tissue sections and microvessels were scanned using a custom built Zeiss 510 meta confocal laser scanning microscope with a Zeiss Apochromat 25x/0.8 NA or C-Apochromat 40x/1.2 NA water immersion objective (Carl Zeiss Microimaging Inc.) We used a 488 nm argon laser to excite Alexa Fluor 488 and Fluorescein, and the emission was collected through a 500-550 nm bp filter; a 543 HeNe laser to excite Alexa fluor 555, Alexa fluor 568 and Cy3 and the emission was collected through a 560-615nm bp filter; a 633 HeNe laser to excite Dylight 649 and the emission was collected through a 650-700 nm bp filter; and a 800 nm tuned femtosecond pulse Tai:Sapphire multiphoton laser was used to excite Hoechst and the emission was collected through a 435-485 nm bp filter. Images were pseudocolored using ZEN software (Carl Zeiss Microimaging, Inc.)

In vitro gelatin zymography

Apoe^{-/-} pericytes were isolated and cultured in 6-well plates as described above. The cells were treated with either vehicle control, astrocytes-derived lipidated apoE4 or apoE3 (40 nM) in the presence of either control siRNA or si*Lrp1* for 48 h, cyclosporine A (50 ng/ml) or PDTC (20 μ M) for 48 h. Next, the condition media (1.5 mL) was concentrated to 20~30 uL with microcon spin columns (Millipore, Bedford, MA) and analyzed by gelatin zymography, as described above.

MMP-9 QPCR

Apoe^{-/-} pericytes were isolated and cultured in 6-well plates as described above. The cells were treated with either vehicle control, astrocytes-derived lipidated apoE4 or apoE3 (40 nM) in the presence of either control siRNA or si*Lrp1* for 48 h, cyclosporine A (50 ng/ml) or PDTC (20 μ M) for 48 h. *Mmp9* mRNA levels were determined by isolating total mRNA with the RNeasy Mini kit (Qiagen Inc). The mRNA was then reverse-transcribed to cDNA using the iScript cDNA Synthesis kit (Bio-Rad, Hercules). The following primers were used for amplification: mouse *MMP-9*, sense 5'- CGAACTTCGACACTGACAAGAAGT -3', anti-sense 5'- GCACGCTGGAATGATCTAAGC -3'. Quantitative PCR was performed using iQ SYBR Green Supermix (Bio-Rad) and IQ4 multicolor detection QPCR system (Bio-Rad). The relative abundance of mouse MMP-9 mRNA was normalized to GAPDH mRNA (determined as described above).

In vivo siRNA infusion

We performed siRNA-mediated knockdown of MMP-9, MMP-2, RELA and LRP1 by infusing their respective siRNA in the hippocampus of *APOE4* transgenic mice or *APOE3* transgenic mice, respectively, using a similar technique as previously published for silencing of LRP1 in the mouse brain²⁶. Briefly, a cannula was stereotactically placed into the hippocampus and one microliter of either control siRNA (Dharmacon, D-001910-10-05), si*Mmp-9* (Dharmacon, E-065579-00-0010), si*Mmp-2* (Dharmacon, E-047467-00-0010) or si*Rela* (Dharmacon, E-040776-00-0010. Fifty μ M of the respective siRNA dissolved in artificial cerebrospinal fluid was slowly infused over 1 hour on two consecutive days in *APOE4* transgenic mice. Using the same procedure, we infused control siRNA or si*Lrp1* (Dharmacon, E-040764-00-0010) into the hippocampus of *APOE3* transgenic mice. Protein expression analysis, immunostaining of cytospun microvascular preparation or cadaverine leakage/cellular uptake assays were performed 72 hours after the first siRNA injection as described above.

Voltage sensitive dye (VSD) imaging

In vivo voltage sensitive dye (VSD) imaging was performed as previously described⁴⁸. A cranial window was placed over the somatosensory cortex as described above (please see Multiphoton In Vivo Microscopy Analysis for details). After carefully removing the dura, without causing any cranial bleeding, RH-1692 VSD (Optical Imaging), dissolved in artificial cerebrospinal fluid (aCSF) was applied to the exposed cortex for 120 min. Next the brain was washed with aCSF, covered with low-melt agarose dissolved in aCSF (~1.3%), sealed with a glass coverslip as described above and the skull was secured to a custom-built microscopy frame. Images were collected using a 12-bit Pixelfly CCD camera coupled to CamWare 3.0 image acquisition Software. RH-1692 was excited using a 627 nm red LED light source and imaged using a custom-built Olympus 2x epifluorescent microscope. Images were collected for 500 ms before and after a mechanical deflection of the hind limb 5 ms in duration. The responses were averaged from 10-20 trials per animal. To correct for any differences in background fluorescence, breathing artifact and/or dye photobleaching, stimulation trial signals were divided by baseline signal profiles collected in the absence of stimulation. The change in fluorescent VSD signal was calculated as a percent change by dividing the signal intensity after stimulation by the average intensity taken before stimulation. The signal intensity was quantified by placing a circular region area of interest over the hind limb region using NIH Image software. The images presented were pseudo-colored to enhance visualization of signal changes using a custom NIH Image J macro. Hind limb coordinates were confirmed in several animals using intrinsic optical signal imaging (data not shown).

Neuritic density analysis

Neuritic density analysis in the cortex and hippocampus was performed as we have previously described¹⁴. Acetone fixed tissue sections were prepared as described above and incubated with mouse anti-SMI-32 (Abcam, ab28029, 1:1000) using the M.O.M kit (Vector Laboratories) followed by incubation with Alexa fluor 488-conjugated streptavidin (Invitrogen, S11223, 1:1000). In order to quantify the SMI-32-positive neuritic density, SMI-32 positive immunofluorescent signal obtained from the cortex and stratum radiatum of the CA1 hippocampal region were subjected to threshold processing using Image J software. The areas occupied by the signal were then analyzed by a blinded investigator using the Image J Area measurement tool. Total SMI-32-positive area was expressed as a percentage of total brain area in each field. In each animal 6 randomly selected fields from the cortex and 4 randomly selected fields from the stratum radiatum region of the stratum radiatum of the CA1 hippocampal region were analyzed in 6 nonadjacent sections (~100 μm apart). Four to six animals per group were analyzed.

Statistical analysis

Data were analyzed by multifactorial analysis of variance (ANOVA) followed by Tukey posthoc tests and Pearson's correlation analysis. A *P* value less than 0.05 was considered statistically significant in all studies.

Methods for data presented in Supplementary Discussion

Lipid profile analysis

The total cholesterol and HDL-cholesterol levels in plasma were analyzed using commercial kits Cat # 439-17501 and 431-52501, Wako Diagnostics) according to the manufacturer's instructions. A triglyceride assay kit (Cat. No. 10010303, Cayman Chemical Company) was used to determine plasma triglyceride levels.

Analysis of physiological parameters

Mean arterial blood pressure, systolic pressure, diastolic pressure and pulse pressure was monitored via the cannulated right femoral artery using a pressure transducer (AD Instruments). The pH levels and blood gases

were determined from a small sample (~90 μ L) of arterial blood, collected from the cannulated right femoral artery, using the Radiometer ABL 77 (Copenhagen). For respiration rate the number of breaths was counted over a 60 s interval and then averaged from three individual trials.

SUPPLEMENTARY DISCUSSION

Lipid profile (includes Table S2, see below)

Several previous studies have reported total cholesterol levels in the transgenic mouse lines used in our study, and some additionally reported triglyceride levels, all in mice fed a normal diet. For instance, a 5 to 8-fold increase in cholesterol levels have been shown in *Apoe*^{-/-}, GFAP-*APOE3* and GFAP-*APOE4* transgenic mice compared to wild type mice, and/or knock-in TR-*APOE3* and TR-*APOE4* transgenic mice⁴⁹⁻⁵¹. Moreover, it has been reported that there are no significant differences in triglyceride levels between wild type, TR-*APOE3* and TR-*APOE4* mice¹⁶. Triglyceride levels were also highly elevated in *Apoe*^{-/-} mice⁵².

Supplementary Table S2 shows plasma lipid profiles in all transgenic mouse lines studied suggesting that the lipid profile in apoE transgenic mice fed normal diet does not influence the BBB phenotype. For instance, similar, substantial increases in total plasma cholesterol levels and non-HDL cholesterol were found in GFAP-*APOE3* and GFAP-*APOE4* mice, but we only found the disrupted BBB and diminished CBF in GFAP-*APOE4* transgenic mice; GFAP-*APOE3* mice had a completely normal cerebrovascular phenotype in spite of similarly increased cholesterol and non-HDL cholesterol levels. Next, TR-*APOE4* transgenic mice had one to two orders of magnitude lower plasma cholesterol and non-HDL cholesterol levels compared to GFAP-*APOE4* transgenic mice, yet both mouse lines had a comparable vascular phenotype with the BBB breakdown and diminished CBF, as we show. Another example is that although TR-*APOE4* and TR-*APOE3* transgenic mice had comparable low triglyceride levels, only *APOE4* transgenics had BBB breakdown and vascular phenotype.

To the best of our knowledge not much information is available in the literature in terms of experimental brain data in apoE transgenic mouse lines fed high-fat, cholesterol-rich diet, except that very old *Apoe*^{-/-} mice (i.e., at 17 months of age) when treated briefly with the high-fat diet (i.e., for 7 weeks) develop macrophage-infiltrated lipid-rich cerebral lesions termed cerebral xanthomas⁵³. More work is needed to determine how high-fat diet influences development of brain lesions including vascular phenotype in apoE4 and other apoE transgenic mice.

Table S2. Plasma lipid profiles in different transgenic mice fed a normal diet.

All values are mean \pm s.e.m., n=3 mice per group

Genotype	Total Cholesterol (mg/dL)	HDL-cholesterol (mg/dL)	Non-HDL cholesterol (mg/dL)	Triglycerides (mg/dL)
<i>Apoe</i> ^{+/+}	73 \pm 2	54 \pm 4	19 \pm 6	28 \pm 1
<i>Apoe</i> ^{-/-}	428 \pm 98	15 \pm 5	413 \pm 101	36 \pm 8
<i>Apoe</i> ^{-/-} <i>Ppia</i> ^{-/-}	361 \pm 27	23 \pm 3	338 \pm 25	54 \pm 8
GFAP- <i>APOE3</i>	554 \pm 65	17 \pm 6	537 \pm 65	58 \pm 10
GFAP- <i>APOE4</i>	436 \pm 20	18 \pm 3	417 \pm 21	36 \pm 2
TR- <i>APOE3</i>	42 \pm 8	34 \pm 7	8 \pm 4	20 \pm 1
TR- <i>APOE4</i>	44 \pm 4	28 \pm 6	16 \pm 2	16 \pm 2

Physiological status (includes Table S3, see below)

Supplementary Table S3 shows that physiological parameters including mean arterial blood pressure, systolic pressure, diastolic pressure and pulse pressure, the heart rate, the respiration rate, the pH levels and blood gasses (pCO₂ and pO₂) were not significantly altered between *Apoe*^{-/-}, wild type, GFAP-*APOE3*, GFAP-*APOE4*, TR-*APOE3*, and TR-*APOE4* mouse lines.

Table S3. Physiological parameters in the different transgenic mice studied

All values are mean \pm s.e.m. from n = 4-6 animals per group. No significant differences were found.

Genotype	<i>Apoe</i> ^{+/+}	<i>Apoe</i> ^{-/-}	TR- <i>APOE3</i>	TR- <i>APOE4</i>	GFAP- <i>APOE3</i>	GFAP- <i>APOE4</i>	<i>Apoe</i> ^{-/-} ; <i>Ppia</i> ^{-/-}
Mean arterial blood pressure (mmHg)	85 \pm 4	87 \pm 6	83 \pm 3	83 \pm 3	84 \pm 4	87 \pm 6	86 \pm 5
Systolic pressure (mmHg)	92 \pm 2	93 \pm 4	89 \pm 4	91 \pm 3	94 \pm 2	94 \pm 2	92 \pm 2
Diastolic pressure (mmHg)	75 \pm 3	76 \pm 4	73 \pm 4	74 \pm 3	76 \pm 4	78 \pm 6	77 \pm 5
Pulse pressure (mmHg)	16 \pm 2	18 \pm 2	16 \pm 3	18 \pm 6	17 \pm 2	16 \pm 5	15 \pm 3
Heart rate (beats/min)	436 \pm 25	419 \pm 22	460 \pm 25	445 \pm 29	457 \pm 17	436 \pm 25	434 \pm 35
Respiration rate (per min)	162 \pm 13	171 \pm 12	164 \pm 18	169 \pm 12	157 \pm 16	164 \pm 16	169 \pm 14
pH	7.25 \pm 0.06	7.27 \pm 0.03	7.25 \pm 0.05	7.26 \pm 0.04	7.28 \pm 0.03	7.25 \pm 0.05	7.25 \pm 0.06
pCO ₂ (mmHg)	43 \pm 4	42 \pm 3	43 \pm 2	42 \pm 3	42 \pm 3	43 \pm 2	42 \pm 3
pO ₂ (mmHg)	93 \pm 3	87 \pm 5	86 \pm 3	88 \pm 3	87 \pm 3	86 \pm 5	87 \pm 3

SUPPLEMENTARY REFERENCES

31. J. A. Piedrahita *et al.*, *Proc. Natl. Acad. Sci. U.S.A.* **89**, 4471-4475 (1992).
32. Y. Sun *et al.*, *J. Neurosci.* **18**, 3261-3272 (1998).
33. J. Colgan, *Genomics* **68**, 167-178 (2000).
34. Famiglio L, *et al.*, *Transplantation* **48**, 316-21 (1989).
35. D. Zhu *et al.*, *Blood* **115**, 4963-4672 (2010).
36. Z. Wu *et al.*, *Nat Med* **11**, 959-65 (2005).
37. E. A. Winkler, R. D. Bell, B. V. Zlokovic, *Mol. Neurodegener.* **5**, 32-42 (2010).
38. K. Maeda, G. Mies, L. Olah, K. A. Hossmann, *J. Cereb. Blood Flow Metab.* **20**, 10-14 (2000).
39. P. Dore-Duffy, A. Katychew, X. Wang, E. Van Buren, *J. Cereb. Blood Flow Metab.* **26**, 613-624 (2006).
40. M. Morikawa *et al.*, *Neurobiol. Dis.* **19**, 66-76 (2005).
41. Deane, R., *et al.*, *Neuron* **43**, 333-344 (2004).

42. R. D. Bell *et al.*, *J. Cereb. Blood Flow Metab.* **27**, 909-918 (2007).
43. R. D. Bell *et al.*, *Nat Cell Bio.* **11**, 143-153 (2009).
44. Fujiyoshi, M., *et al.*, *J Neurochem.* **118**,407-15 (2011).
45. Zlokovic, B.V., *et al.*, *Proc Natl Acad Sci U S A* **93**, 4229-4234 (1996).
46. Morales, C.R., *et al.*, *J Histochem Cytochem* **54**, 1115-1127 (2006).
47. Ranganathan, S., Knaak, C., *J Biol Chem* **274**, 5557-5563 (1999).
48. C. E. Brown *et al.*, *J. Neurosci.* **29**, 1719-1734 (2009).
49. P.M. Sullivan *et al.*, *Neuroscience* **124**, 725-733 (2004).
50. P.M. Sullivan *et al.*, *J. Biol. Chem.* **272**, 17972-17980 (1997).
51. J.D. Smith *et al.*, *Neurobiol. Aging* **19**, 407-413 (1998).
52. V.S. Kashyap *et al.*, *J. Clin. Invest.* **96**, 1612-1620 (1995).
53. L.C. Walker *et al.*, *Am. J. Pathol.* **151**, 1371-1377 (1997).